### 5-Halogenation of Uridine Suppresses Protonation-Induced Tautomerization and Enhances Glycosidic Bond Stability of Protonated Uridine: Investigations via IRMPD Action Spectroscopy, ER-CID Experiments, and Theoretical Calculations

Neven N. Mikawy, <sup>a</sup> H. A. Roy, <sup>a</sup> E. Israel, <sup>a</sup> L. A. Hamlow, <sup>a</sup> Y. Zhu, <sup>a</sup> G. Berden, <sup>b</sup> J. Oomens, <sup>b</sup> C. E. Frieler, <sup>a</sup> and M. T. Rodgers\*, <sup>a</sup>

#### **ABSTRACT**

Uridine (Urd), a canonical nucleoside of RNA, is the most commonly modified nucleoside among those that occur naturally. Uridine has also been an important target for the development of modified nucleoside analogues for pharmaceutical applications. In this work, the effects of 5halogenation of uracil on the structures and glycosidic bond stabilities of protonated uridine nucleoside analogues are examined using tandem mass spectrometry and computational methods. Infrared multiple photon dissociation (IRMPD) action spectroscopy experiments and theoretical calculations are performed to probe the structural influences of these modifications. Energyresolved collision-induced dissociation experiments along with survival yield analyses are performed to probe glycosidic bond stability. The measured IRMPD spectra are compared to linear IR spectra predicted for the stable low-energy conformations of these species computed at the B3LYP/6-311+G(d,p) level of theory to determine the conformations experimentally populated. Spectral signatures in the IR fingerprint and hydrogen-stretching regions allow the 2,4-dihydroxy protonated tautomers (T) and O4- and O2-protonated conformers to be readily differentiated. Comparisons between the measured and predicted spectra indicate that parallel to findings for uridine, both T and O4-protonated conformers of the 5-halouridine nucleoside analogues are populated, whereas O2-protonated conformers are not. Variations in yields of the spectral signatures characteristic of the T and O4-protonated conformers indicate that the extent of protonation-induced tautomerization is suppressed as the size of the halogen substituent increases. Trends in the energy-dependence of the survival yield curves find that 5-halogenation strengthens the glycosidic bond, and that the enhancement in stability increases with the size of the halogen substituent.

**Keywords.** Uridrine, 5-Halouridine nucleoside analogues, Infrared multiple photon dissociation (IRMPD) action spectroscopy, Energy-resolved collision-induced dissociation (ER-CID), Survival yield analysis.

Corresponding author: M. T. Rodgers, mrodgers@chem.wayne.edu, Tel. (313)577-2431

<sup>&</sup>lt;sup>a</sup> Department of Chemistry, Wayne State University, Detroit, MI, 48202, USA <sup>b</sup> Radboud University, Institute for Molecules and Materials, FELIX Laboratory, Toernooiveld 7, 6525ED Nijmegen, The Netherlands

#### INTRODUCTION

The higher-order (secondary, tertiary, and quaternary) structures of DNA and RNA nucleic acids are strongly influenced by the sequence and conformations of their nucleoside building blocks. Thus, the determination of nucleoside conformation and how it is influenced by the local environment is important to understand both static and dynamic nucleic acid structures. The nucleoside building blocks comprise a pyrimidine (cytosine, thymine, or uracil) or purine (adenine or guanine) nucleobase and a five-carbon (2'-deoxyribose or ribose) sugar, connected via a N-glycosidic (C1'–N1 or C1'–N9) bond. The stability of these N-glycosidic bonds is vital as they must be stable enough to preserve the proper sequence (i.e., the genetic code) of DNA and RNA strands as well as the various intracellular mechanisms employed upon this code to allow for replication to occur during new cell growth and the transfer of genetic information during reproduction to foster the stable continuation of life. However, these N-glycosidic bonds must also be susceptible to cleavage to correct damaged or undesirably mutated nucleobases and to salvage nucleobase moieties during the degradation of DNA and RNA.<sup>1–8</sup>

Nucleoside modifications (to the nucleobase and/or sugar moieties) have been found to alter their structures, influence their base-pairing and binding interactions, and affect the stabilities of their N-glycosidic bonds. Although DNA and RNA nucleic acids employ a mere four-letter (nucleobase) genetic code, both make use of modifications to enhance their functionalities. DNA employs fewer than two dozen modifications, which play roles in immunity and epigenetic control of gene expression. In contrast, the chemical and structural diversity and the extent of post-transcriptional modification of RNA is extraordinary. Presently, there are 152 different naturally occurring and many more synthetically modified nucleosides known. Naturally and synthetically-modified nucleosides have proven to be effective antiviral and anticancer therapies for various diseases. Uridine (Urd), one of the canonical nucleosides of RNA, is the most commonly modified nucleoside among those that occur naturally. And thus, it naturally follows that uridine has also been an important target for the synthesis and development of modified nucleoside analogues for pharmaceutical applications. Uracil (Ura), the nucleobase of Urd, possesses two keto

moieties that may be susceptible to tautomerization depending upon the local environment, and thus provides a handle for altering the properties of uridine nucleosides. Tautomerization of uracil, occurs readily upon protonation, resulting in the 2,4-dihydroxy tautomer.<sup>18–22</sup> Protonation induced tautomerization has also been observed for several modified uracils including 5-methyluracil (thymine), 5-halouracils, 2-thiouracil, 4-thiouracil, and 2,4-dithiouracil.<sup>20–22</sup> Likewise, protonation-induced tautomerization has also been observed for uridine nucleoside analogues including 5-methyluridine (thymidine, Thd), 5-methyl-2'-deoxyurdine (dThd)<sup>23</sup> and several modified at the 2'-position of the ribose moiety including 2'-deoxyuridine (dUrd), 2',3'-dideoxyuridine (ddUrd), 2'O-methyluridine (Urdm), 2'-O-methyl-5-methyluridine (dThdm), 2'-fluorouridine (Urdfl), and uracil arabinoside (araUrd).<sup>24-28</sup> This unique character of protonated uracil suggests that a variety of conformations may be accessible to protonated uridine, [Urd+H]<sup>+</sup>, and its analogues. Indeed, combined IRMPD action spectroscopy and computational work has established that a diverse mixture of 2,4-dihydroxy tautomers and either O4- and/or O2-protonated conformers are populated by these uridine nucleoside analogues when generated by electrospray ionization.<sup>23-28</sup>

Halogenation is a common modification employed in pharmaceutical studies that enables systematic variation in the electronic properties of the molecule of interest due to the availability of halogen substituents that vary in size, polarizability, and electron withdrawing properties. Halogen-substituted nucleosides and related compounds have been shown to exhibit interesting chemotherapeutic, biochemical, and biophysical properties. Pational variation of the C5-substituent of uridine nucleosides can enhance their properties in terms of oral bioavailability, metabolic stability, and pharmacokinetics. 5-Halouridine nucleoside analogues are of great pharmaceutical interest and have been investigated extensively as antineoplastic and antiviral agents. Several 5-chlorouridine nucleoside analogues are less cytotoxic and they along with 5-bromouridine exhibit selective antiviral activity to human immunodeficiency virus (HIV). Alogenated uridine nucleoside analogues are important intermediates for the synthesis of a wide range of modified nucleosides showing activity, mainly against herpes simplex virus type 1 and 2

and varicella-zoster virus. Radioactive 5-halogenated uridine nucleoside analogues have also been used as mechanistic probes for DNA metabolism studies and in RNA labeling studies.<sup>29,32</sup>

To elucidate the influence of 5-halogenation on the structure and stability of the protonated form of Urd, synergistic spectroscopic, mass spectrometric, and theoretical studies of the protonated forms of the 5-halouridines ( $x^5$ Urd) were performed here, where  $x^5$ Urd = 5fluorouridine (fl<sup>5</sup>Urd), 5-chlorouridine (cl<sup>5</sup>Urd), 5-bromouridine (br<sup>5</sup>Urd), and 5-iodouridine (io<sup>5</sup>Urd). Infrared multiple photon dissociation (IRMPD) action spectra of the protonated forms of the 5-halouridines,  $[x^5\text{Urd+H}]^+$ , were measured over the IR fingerprint and hydrogen-stretching regions. Complementary electronic structure calculations were performed to determine the stable low-energy conformations available to these species and to predict their IR spectra. Comparative analyses of the measured IRMPD and predicted IR spectra were performed to elucidate the preferred sites of protonation, and the low-energy tautomeric conformations that were populated in the experiments. Energy-resolved collision-induced dissociation (ER-CID) experiments of the protonated forms of  $[Urd+H]^+$  and the 5-halouridines,  $[x^5Urd+H]^+$ , were also performed. Survival yield analyses of the ER-CID behavior were performed to elucidate the relative glycosidic bond stabilities of these species. Comparisons among these systems and to results previously reported for the protonated form of uridine, [Urd+H]<sup>+</sup>, provide insight into the influence of the 5-halogen substituent on the structures, IR signatures, and glycosidic bond stabilities of the 5-halouridine nucleoside analogues.

#### EXPERIMENTAL AND COMPUTATIONAL SECTION

#### **Materials**

Uridine and the 5-halogenated uridine nucleoside analogues were purchased from Sigma-Aldrich (St. Louis, MO, USA). The HPLC grade methanol, water, and hydrochloric acid used for the IRMPD action spectroscopy experiments were purchased from Sigma Aldrich (Zwijndrecht, The Netherlands). The HPLC grade water used for the ER-CID measurements was purchased from Sigma Aldrich (St. Louis, MO, USA). The HPLC grade methanol and ammonium acetate used for

the ER-CID measurements was purchased from Fisher Scientific Company (St. Fair Lawn, NJ, USA).

#### **IRMPD Action Spectroscopy Experiments**

IRMPD action spectra of the protonated forms of the 5-halouridines,  $[x^5Urd+H]^+$ , where  $x^5$ Urd = fl<sup>5</sup>Urd, cl<sup>5</sup>Urd, br<sup>5</sup>Urd, and io<sup>5</sup>Urd were measured using a 4.7 T Fourier transform ion cyclotron resonance mass spectrometer (FT-ICR MS)<sup>33–35</sup> coupled to the FELIX free electron laser (FEL, 10 Hz rep rate, bandwidth 0.3% of central frequency, energy up to 70 mJ/pulse)<sup>36</sup> or an OPO/OPA laser system (10 Hz rep rate, 3 cm<sup>-1</sup> bandwidth, energy up to 20 mJ, from LaserVision, Bellevue, WA, USA) that is pumped by a Nd:YAG laser (InnoLas SpitLight 600, Krailling, Germany). Hydrochloric acid and HPLC grade methanol and water were used to prepare working solutions for each 5-halouridine nucleoside analogue. 1 mM Urd or x<sup>5</sup>Urd along with 10 mM HCl were dissolved in a 50%:50% (v/v) methanol: water mixture to facilitate formation of  $[x^5Urd+H]^+$ . The analyte solutions were delivered to a "Z-spray" ESI source (Micromass, Milford, MA, USA) at a flow rate in the range of 3.0–8.8 µL min<sup>-1</sup>. Ions emanating from the source were accumulated in a rf hexapole ion trap for several seconds to bring about thermalization of the trapped ion population. The ions were then pulsed-extracted from the hexapole into a quadrupole deflector and injected into the ICR cell via a 1-m long rf octopole ion guide. To preserve the room temperature distribution of the ions as they were extracted from the hexapole, electrostatic switching of the dc bias of the octopole (in the absence of a pulse of buffer gas) was employed.<sup>34</sup> The [x<sup>5</sup>Urd+H]<sup>+</sup> ions were isolated using stored waveform inverse Fourier transform (SWIFT) techniques. The  $[x^{5}\text{Urd}+H]^{+}$  ions were irradiated for 2.5–3 s by the FEL over the IR fingerprint region between  $\sim$ 700 and  $\sim$ 1900 cm<sup>-1</sup> or for 5–10 s by the OPO/OPA laser system over the range between  $\sim$ 3300 and ~3800 cm<sup>-1</sup> to characterize their photodissociation behavior. The IRMPD yield was calculated for each protonated nucleoside, from its signal magnitude, and the sum of the signal magnitudes of the product ions, after laser irradiation at each vibrational frequency as shown in eq 1.

IRMPD yield = 
$$(\sum_{i} I_{f_i})/(I_p + \sum_{i} I_{f_i})$$
 (1)

The IRMPD yield was normalized linearly to correct for changes in the output of the laser as a function of the frequency of the FEL or OPO lasers. The IRMPD yield was plotted versus the irradiation frequency thus producing the IRMPD action spectrum.

#### **ER-CID Experiments**

ER-CID experiments of the protonated forms of Urd,  $[\text{Urd+H}]^+$ , and the 5-halouridines,  $[x^5\text{Urd+H}]^+$ , where  $x^5\text{Urd} = \text{fl}^5\text{Urd}$ ,  $\text{cl}^5\text{Urd}$ ,  $\text{br}^5\text{Urd}$ , and  $\text{io}^5\text{Urd}$  were performed using an amaZon ETD quadrupole ion trap mass spectrometer (QIT MS, Bruker Daltonics, Bremen, Germany). Ammonium acetate and HPLC grade methanol and water were used to prepare working solutions for each uridine nucleoside analogue. 5  $\mu$ M Urd or  $x^5$ Urd along with 0.5% (v/v) ammonium acetate were dissolved in a 50%:50% (v/v) methanol: water mixture to facilitate formation of  $[\text{Urd+H}]^+$  and  $[x^5\text{Urd+H}]^+$ . The analyte solutions were introduced into the Apollo ESI source at a flow rate of 3  $\mu$ L/min. Helium, used for both cooling and collisional activation, was introduced into the ion trap at a stagnation pressure of ~1–2 mTorr. The  $q_z$  value for the ER-CID experiments was set to 0.25 to balance the trapping efficiency and low mass cut-off. The rf excitation amplitude was increased from 0.00 V (corresponding to isolation of the precursor ion) to the amplitude required to induce complete dissociation of the precursor ion at a step size of 0.01 V. Each ER-CID experiment was performed in triplicate to assess reproducibility. The CID mass spectra were acquired using Compass Data Analysis 4.0 (Bruker Daltonics, Bremen, Germany).

#### **Survival Yield Analyses**

Survival yield analysis is a robust method to determine the relative stabilities of precursor ions.<sup>27,37-47</sup> For the ER-CID experiments of protonated uridine and the 5-halouridines nucleoside analogues, the survival yield of the precursor ion was calculated at each rf excitation amplitude examined using eq 2,<sup>48</sup>

Survival yield = 
$$I_p/(I_p + \sum_i I_{f_i})$$
 (2)

where  $I_p$  and  $(I_p + \sum_i I_{f_i})$  are defined as in eq 1. The survival yields were calculated using custom software developed in our laboratory. A survival yield curve was generated for each system by plotting the survival yield as a function of the rf excitation amplitude. The CID<sub>50%</sub> value, i.e., the

rf excitation amplitude required to produce dissociation of 50% of the precursor ions, was determined using four parameter logistic dynamic fitting based on eq 3,

Survival Yield = 
$$min + \frac{max - min}{1 + \left(\frac{rf_{EA}}{CID_{50\%}}\right)^{CID_{slope}}}$$
 (3)

where *max* is the maximum possible value of the survival yield (1) and corresponds to isolation of the precursor ion without fragmentation; *min* is the minimum possible value of the survival yield (0) and corresponds to complete dissociation of the precursor ion; rf<sub>EA</sub> is the rf excitation amplitude applied; and CID<sub>slope</sub> is the slope of the declining region of the survival yield curve. The relative stabilities of protonated Urd and the 5-halouridines nucleoside analogues were elucidated by comparing the CID<sub>50%</sub> values determined for these systems. Because the fragmentation pathways of these uridine nucleosides involve solely N-glycosidic bond cleavage, the CID<sub>50%</sub> values can be directly correlated with the relative N-glycosidic bond stabilities of these nucleoside analogues. Data analyses were performed using Sigma Plot 10.0 (Systat Software, Inc., San Jose, CA, USA).

#### **Computational Details**

The chemical structures of neutral uridine and the 5-halouridine nucleoside analogues are compared in Figure 1. The most favorable protonation sites/tautomeric states for Urd were previously established as O2 and O4 as well as the 2,4-dihydroxy protonated tautomers.<sup>24</sup> Therefore, the O2- and O4-protonated forms as well as the 2,4-dihydroxy protonated tautomers of the  $[x^5\text{Urd}+\text{H}]^+$  species are examined here as well. In that work, it was also established that the conformers of  $[\text{Urd}+\text{H}]^+$  populated in the experiments are all ring-closed structures as the predicted IR spectra of ring-open conformers exhibit obvious differences from the measured IRMPD spectrum that clearly eliminate their presence from the experimental population.<sup>24</sup> Therefore, the sugar moieties of the  $[x^5\text{Urd}+\text{H}]^+$  species examined here were also limited to their ring-closed forms. Candidate structures for each neutral and protonated form of Urd and the  $x^5\text{Urd}$  nucleoside analogues were generated by simulated annealing using HyperChem software<sup>49</sup> with the Amber 3 force field. Each initial structure of Urd,  $[\text{Urd}+\text{H}]^+$ , and the 5-halogenated nucleoside analogues

of these species was subjected to 300 cycles of simulated annealing. Each cycle involved 0.3 ps of thermal heating from 0 to 1000 K, 0.2 ps of sampling of conformational space at 1000 K, the simulation temperature, and 0.3 ps of thermal cooling from 1000 to 0 K. The resulting structure at the end of each cycle was optimized to a local minimum using the Amber 3 force field. A molecular mechanics (MM) calculation was performed every 1 fs in each cycle, and a snapshot of the lowest energy structure found at the end of each cycle was saved and used as the initial conformation for the subsequent cycle. Approximately 30 of the 300 candidate structures of the neutral and each protonated form of Urd and the x<sup>5</sup>Urd nucleoside analogues were chosen for higher level optimization based primarily on their relative stabilities predicted via the simulated annealing procedure. To ensure that conformational space was comprehensively explored, additional structures were examined to ensure that all possible combinations of protonation site/tautomeric state (O2, O4, and the 2,4-dihydroxy tautomers), nucleobase orientation (anti and syn), and sugar puckering (C2'-endo, C3'-endo, C2'-exo and C3'-exo) found in the simulated annealing processes were included. Geometry optimizations, frequency analyses, and single point energy calculations of all candidate structures chosen were performed using the Gaussian 16 suite of programs.<sup>50</sup> To facilitate convergence of the geometry optimization, all candidate structures were first optimized at the B3LYP/6-31G(d) level of theory. The stable structures thus determined were then reoptimized at the B3LYP/6-311+G(d,p) level to improve the description of the intramolecular hydrogen-bonding interactions that stabilize these systems. The B3LYP/6-311+G(d,p) level of theory was also used to perform frequency analyses of the optimized structures. Single point energies were calculated at the B3LYP/6-311+G(2d,2p) level of theory to predict the relative stabilities of the low-energy conformers. Zero-point energy (ZPE) and thermal corrections to 298 K based on the vibrational frequencies calculated at the B3LYP/6-311+G(d,p) level of theory were included in the relative stabilities determined. Linear IR spectra based on these vibrational frequencies, scaled by a factor of 0.98 and broadened using a 20 cm<sup>-1</sup> fwhm Gaussian line shape over the IR fingerprint region, and scaled by a factor of 0.955 with 15 cm<sup>-1</sup> broadening for the hydrogen-stretching region, along with the computed IR intensities were generated for all stable

conformations computed. When interpreting the IRMPD spectra via comparisons with the calculated IR spectra, one should keep in mind that the measured nonlinear IRMPD and calculated linear IR spectra are not identical. Multiple photons are involved in the IRMPD processes, which may lead to varying degrees of anharmonicity among different vibrational modes. Therefore, there are inevitable differences between the measured IRMPD and calculated IR spectra including spectral broadening, changes in the relative intensities of IR bands, and even shifts in the band positions due to variable anharmonicities and the efficiency of intramolecular vibrational redistribution (IVR) of the various modes of the system. However, these discrepancies are generally sufficiently limited that the IRMPD spectrum still provides a good reflection of the linear IR absorption spectrum.<sup>51</sup>

#### **RESULTS**

#### **IRMPD Action Spectroscopy**

The primary (only) photodissociation pathway observed for the  $[x^5\text{Urd+H}]^+$  ions involves N-glycosidic bond cleavage producing the corresponding protonated 5-halouracil,  $[x^5\text{Ura+H}]^+$ , as the ionic product detected as described by reaction 4.

$$[x^{5}\text{Urd}+\text{H}]^{+} \xrightarrow{n \text{ hv}} [x^{5}\text{Ura}+\text{H}]^{+} + (x^{5}\text{Urd}-x^{5}\text{Ura})$$
(4)

Here, the neutral loss corresponds to the ribosyl sugar moiety minus the C2' $\alpha$  proton (i.e., C<sub>5</sub>H<sub>8</sub>O<sub>4</sub>), which is transferred to the departing uracil nucleobase upon dissociation. The measured IRMPD action spectra for [Urd+H]<sup>+24</sup> and the [ $x^5$ Urd+H]<sup>+</sup> nucleoside analogues are compared in Figure 2. All five IRMPD spectra exhibit many parallel spectral signatures, but also exhibit sufficient differences including small shifts in the band positions and variations in the relative peak intensities and widths such that [Urd+H]<sup>+</sup> and the [ $x^5$ Urd+H]<sup>+</sup> nucleoside analogues are readily differentiated.

In the fingerprint region from ~700 to 1000 cm<sup>-1</sup>, a number of very weak features are barely discernible from the noise in the spectra of [Urd+H]<sup>+</sup> and [fl<sup>5</sup>Urd+H]<sup>+</sup>, however as the size of the 5-halogen substituent increases two features at ~760 and 870 cm<sup>-1</sup> emerge and increase in intensity.

Three relatively intense spectral features are observed in the region from ~1000–1300 cm<sup>-1</sup>; the most intense of these three features is observed at ~1100 cm<sup>-1</sup> and its position is unaffected by the 5-substituent. The next most intense feature is observed at ~1200 cm<sup>-1</sup> in the spectrum of [Urd+H]<sup>+</sup> but shifts slightly to the red upon 5-halogenation. The least intense of these features is observed at ~1275 cm<sup>-1</sup> and appears as a shoulder of the feature at ~1200 cm<sup>-1</sup> in the spectra of [Urd+H]<sup>+</sup> and [fl<sup>5</sup>Urd+H]<sup>+</sup>, however as the size of the 5-halogen substituent increases this feature grows in intensity and shifts slightly to the red. Two minor features are observed at ~1380 and 1440 cm<sup>-1</sup> in the spectrum of [Urd+H]<sup>+</sup>; these features shift slightly to the red upon 5-halogenation and the intensity of the first feature decreases as the size of the substituent increases. Three relatively intense features are observed at ~1505, 1595, and 1650 cm<sup>-1</sup> in the spectrum of [Urd+H]<sup>+</sup>. The intensity of the first feature increases upon 5-fluorination, but then decreases as the size of the 5-halogen substituent increases. In contrast, the latter two features decrease upon 5-fluorination, but then increase as the size of the 5-halogen substituent increases. A single feature is observed at ~1800 cm<sup>-1</sup> in all five spectra; the intensity of this feature decreases upon 5-fluorination, but then increases in magnitude as the size of the halogen substituent increases.

Five spectral features are observed in the hydrogen-stretching region of the IRMPD spectrum of [Urd+H]<sup>+</sup> at ~3395, 3510, 3565, 3615, and 3665 cm<sup>-1</sup>. The intensity, but not the band position, of the modest feature at ~3395 cm<sup>-1</sup> varies upon 5-halogenation, decreasing substantially upon 5-fluorination, and then increasing as the size of the halogen substituent increases. The weak feature at ~3500 cm<sup>-1</sup> is unaffected by 5-fluorination (and only seen at the noise level); this feature shifts to the red and increases in intensity for the larger halogen substituents. The intense feature at ~3565 cm<sup>-1</sup> splits into two features at 3557 and 3573 cm<sup>-1</sup> upon 5-halogenation. These features decrease in intensity as the size of the halogen substituent increases. The features at ~3610 and 3665 cm<sup>-1</sup> exhibit a decrease in intensity upon 5-halogenation, but their position are relatively unaffected.

#### **ER-CID Experimental Results**

The CID mass spectra of [Urd+H]+ and the [x5Urd+H]+ analogues acquired at an rf

excitation amplitude near the CID<sub>50%</sub> value are compared in Figure 3. The primary (only) fragmentation pathway observed for  $[Urd+H]^+$  and  $[x^5Urd+H]^+$  involves *N*-glycosidic bond cleavage with the proton retained by the nucleobase (parallel to that observed upon IR irradiation) as summarized in reaction 5.

$$[x^{5}\text{Urd}+H]^{+} \xrightarrow{n \text{ He}} [x^{5}\text{Ura}+H]^{+} + (x^{5}\text{Urd}-x^{5}\text{Ura})$$
 (5)

The CID pathway described by reaction 6 is not observed under "enhanced resolution" conditions (where  $P_{He} = \sim 2$  mTorr within the trap,  $\sim 1.1 \times 10^{-6}$  Torr background), but does occur as a very minor reaction pathway producing a product ion at m/z = 133 when the experiments are performed under "maximum resolution" conditions (where  $P_{He} = \sim 1$  mTorr within the trap,  $\sim 0.56 \times 10^{-6}$  Torr background).

$$[x^{5}\text{Urd}+\text{H}]^{+} \xrightarrow{n \text{ He}} [x^{5}\text{Urd}-x\text{Ura}+\text{H}]^{+} + x^{5}\text{Ura}$$
(6)

No other CID pathways were observed under the experimental conditions employed at any of the rf<sub>EA</sub> values examined.

#### **Theoretical Results**

Despite the diversity of candidate structures subjected to higher-level optimization, only a limited number of stable low-energy structures were found for the neutral and protonated forms of Urd and  $x^5$ Urd as many of the initial structures converged to essentially equivalent optimized structures. The B3LYP/6-311+G(d,p) optimized structures of the stable low-energy conformers (those within ~10–15 kJ/mol of the ground conformer) along with their B3LYP/6-311+G(2d,2p) relative Gibbs energies at 298 K for neutral Urd and the  $x^5$ Urd nucleoside analogues are shown in Figures S1–S5 of the Supporting Information, whereas those of [Urd+H]<sup>+</sup> and [ $x^5$ Urd+H]<sup>+</sup> are shown in Figures S6–S10. The nomenclature used to describe the stable low-energy conformers of the protonated forms of Urd and the  $x^5$ Urd nucleoside analogues is based on the protonation site/tautomeric conformation (T for the 2,4-dihydroxy tautomers, O4 or O2) and is followed by a capital letter or lowercase Roman numeral for each conformer. Capital letters (A, B, C, etc.) are used for conformers that were previously found for both [Urd+H]<sup>+</sup> and [dUrd+H]<sup>+</sup>, whereas lowercase Roman numerals (i, ii, iii, etc.) are used for conformers that were only found for

[Urd+H]<sup>+</sup>.<sup>24</sup> The ordering of the low-energy conformers is based on their B3LYP relative Gibbs energies at 298 K. Specific conformers are indicated in boldface (e.g., **TA**, **Ti**, **O4A**), whereas standard font is used when discussing general types of conformers (i.e., T vs. O4 vs O2).

#### Ground and Stable Low-Energy Conformers of Neutral Urd and x5Urd

The optimized structures of the ground and stable low-energy conformers of Urd and xUrd along with their relative Gibbs energies at 298 K are compared in Figures S1–S5 of the Supporting Information. The key structural parameters, i.e., the pseudorotation phase angles (sugar puckers), glycosidic bond angles, and 5'-hydroxy orientations of these conformers are compared in the polar plots of Figure 4. As can be seen in Figure S1, the ground conformation of Urd exhibits C2'-endo sugar puckering, an anti nucleobase orientation, a gauche<sup>+</sup> 5'-hydroxy orientation, and is stabilized by O3'H···O2'H···O2 dual hydrogen-bonding interactions. All of these geometric features are retained in ground conformations of the  $x^5$ Urd nucleoside analogues except that the pseudorotation phase angle increases such that these conformers exhibit C3'-exo sugar puckering (see Figures S2-S5). The O3'H···O2'H···O2 dual hydrogen-bonding motif found in the ground conformers is common among all of the lowest-energy conformers that exhibit an anti nucleobase orientation, whereas the most stable syn conformers are stabilized by O2'H···O3'H and O5'H···O2 hydrogenbonding interactions. Conformers lacking the O2'H···O2 hydrogen-bonding interaction and stabilized by only a single O2'H···O3'H or O3'H···O2'H hydrogen-bonding interaction lie at least 4.7–10.2 kJ/mol above the corresponding ground conformers. The pseudorotation phase angle (P) of the ground conformer of Urd is 156° (C2'-endo); 5-halogenation results in an increase in P to 183–186°. The pseudorotation phase angles found among the low-energy conformers of Urd span the range from 41-177° corresponding to C4'-exo, O4'-endo, C1'-exo, and C2'-endo sugar puckerings. 5-Halogenation expands the range of P found among the low-energy conformers to  $18-201^{\circ}$  such that in addition to the sugar puckers found for Urd, the  $x^{5}$ Urd analogues also exhibit C3'-endo and C3'-exo sugar puckers. Both anti and syn conformers are represented among the lowenergy conformers of Urd and xUrd, with anti more common and energetically favored over syn conformers. The ground conformer of Urd has a glycosidic bond angle of 180°, which increases to 186° upon 5-halogenation. Glycosidic bond angles in the range of  $61-62^{\circ}$ ,  $69-70^{\circ}$ ,  $180-187^{\circ}$ , and  $242-243^{\circ}$  are represented among the stable low-energy conformers of Urd and  $x^{5}$ Urd, whereas only the  $x^{5}$ Urd analogues have stable conformers with a glycosidic bond angle in the range of  $197-198^{\circ}$ . The 5'-hydroxy orientations of the ground conformers of Urd and the  $x^{5}$ Urd analogues are all gauche<sup>+</sup>. However, gauche<sup>+</sup> ( $285-299^{\circ}$ ), trans ( $41-72^{\circ}$ ), and gauche<sup>-</sup> ( $165-175^{\circ}$ ) orientations of the 5'-hydroxy substituent are all found among the low-energy conformers for Urd and the  $x^{5}$ Urd nucleoside analogues.

#### Ground and Stable Low-Energy Conformers of Protonated Urd and x<sup>5</sup>Urd

The optimized structures of the ground and stable low-energy conformers of [Urd+H]<sup>+</sup> and  $[x^{5}\text{Urd+H}]^{+}$  along with their relative Gibbs energies at 298 K are compared in Figures S6–S10. The pseudorotation phase angles, glycosidic bond angles, and 5'-hydroxy orientations of these conformers are compared in the polar plots of Figure 4. Table 1 lists the 0 and 298 K relative enthalpies and Gibbs energies of these stable low-energy conformers of [Urd+H]<sup>+</sup> and  $[x^{5}\text{Urd+H}]^{+}$ . The relative Gibbs energies of these low-energy conformers are also visually compared in Figure 5. All three sites of protonation/tautomeric forms are represented among the low-energy conformers for all five protonated uridine nucleoside analogues, with T and O4 conformers more common and energetically favored over O2 conformers (see Figure 5). As can be seen in Figure 5, the relative stability of the T vs. O4 (and to a lesser extent the O2) conformers varies with the 5-substituent. The ground Ti conformers are more stable than the most stable O4protonated conformers (O4A) for [Urd+H]<sup>+</sup> and [fl<sup>5</sup>Urd+H]<sup>+</sup> by 2.9 and 6.7 kJ/mol, whereas these conformers are predicted to be of very similar stability for [cl<sup>5</sup>Urd]<sup>+</sup>, 0.0 vs. 0.4 kJ/mol, and the ground O4 conformers are favored over the most stable Ti conformers for [br<sup>5</sup>Urd+H]<sup>+</sup> and [io<sup>5</sup>Urd+H]<sup>+</sup> by 4.9 (**O4A**) and 6.4 kJ/mol (**O4i**), respectively. The **Ti** conformers exhibit C2'-endo sugar puckering with an anti nucleobase orientation and are stabilized by O2H···O2'H···O3' dual hydrogen-bonding interactions and a C2'H···O5' noncanonical hydrogen-bonding (dispersion) interaction. The TA conformer is the next most stable 2,4-hydroxy protonated tautomer for all five protonated uridine nucleoside analogues. Similar to the Ti conformers, the TA conformers also exhibit C2'-endo sugar puckering with an *anti* nucleobase orientation. However, the orientation of the 2-hydroxy substituent differs such that these conformers are only stabilized by a single O2'H···O3' hydrogen-bonding interaction. The noncanonical C2'H···O5' hydrogen-bonding interaction is also maintained, but this change in geometry enables the nucleobase to rotate such that additional stabilization is gained via a C6H···O5' noncanonical hydrogen-bonding interaction. There is almost no energetic trade-off between these stabilizing interactions for [Urd+H]<sup>+</sup> and [ $x^5$ Urd+H]<sup>+</sup>, a mere 0.2, 1.1, 1.1, 1.3, and 0.1 kJ/mol. The **O4A** conformers are highly parallel to the **TA** conformers; they differ only in the tautomeric form of the nucleobase. The most stable O2-protonated conformers (**O2i**) exhibit geometries very similar to the **Ti** conformers except in the tautomeric form of the nucleobase, and are predicted to be less stable than the ground conformers by 8.0, 6.4, 6.1, 6.2, and 7.0 kJ/mol, respectively.

All of the low-energy conformers of the protonated uridine nucleoside analogues are stabilized by either one or two canonical and one or two noncanonical hydrogen-bonding interactions. One hydrogen-bonding interaction is always found between the 2'- and 3'-hydroxy substituents; O2'H···O3' is energetically favored over O3'H···O2'. When the O2 position is protonated as in the T and O2 conformers, two hydrogen-bonding interactions are possible. Conformers that exhibit an *anti* nucleobase orientation may either engage in O2H···O2'H···O3' (Ti, O2i) or O3'H···O2'H···O2 (O4ii) dual hydrogen-bonding interactions, whereas those with a *syn* orientation are stabilized by O2'H···O3' and O2H···O2'H hydrogen-bonding interactions (TC, O2A). All of the stable conformers exhibiting an *anti* orientation are stabilized by a noncanonical C6H···O5' hydrogen-bonding interaction except the Ti and O2i conformers where the dual hydrogen-bonding interactions lock the nucleobase in an orientation that does not allow this interaction to occur. All of the conformers with C2'-endo sugar puckering are also stabilized by a noncanonical C2'H···O5' hydrogen-bonding interaction.

The key geometric parameters of the stable low-energy conformers of  $[Urd+H]^+$  and  $[x^5Urd+H]^+$  are highly parallel (see Figure 4). Notably, protonation reduces the range of pseudorotation phase angles (sugar puckers) and 5'-hydroxy orientations found among the low-

energy conformers of the uridine nucleoside analogues. Virtually all of the low-energy conformers exhibit C2'-endo ( $P = 151-175^{\circ}$ ) or C3'-endo ( $P = 11-17^{\circ}$ ) puckering, with C2'-endo more common and energetically favored over C3'-endo by 2.5, 3.4, 0.8, and 0.5 kJ/mol for all of the protonated uridine nucleoside analogues except [io $^{5}$ Urd+H]<sup>+</sup> where C3'-endo is favored over C2'-endo by 0.6 kJ/mol. Conformers exhibiting other sugar puckerings found via simulated annealing generally lie higher in energy and convert to their more stable C2'-endo or C3'-endo counterparts upon higher-level geometry optimization. However, one stable low-energy C3'-exo ( $P = 198-199^{\circ}$ ) puckered conformer was found for each protonated nucleoside, **O4ii**, which is stabilized by O3'H···O2'H···O2 dual hydrogen-bonding interactions. These C3'-exo conformers are 2.3–11.2 kJ/mol less stable than the corresponding ground T or O4 conformers.

Both *anti* and *syn* conformers are represented among the low-energy structures for all five protonated uridine nucleoside analogues. The range of glycosidic bond angles is similar to that found for the neutral nucleosides with *anti* conformers in the ranges between 182–203° and 226–230° and *syn* conformers in the range of 49–51°, with *anti* more common and energetically favored over *syn* conformers by 2.9–8.6 kJ/mol. One T (TC) and one O2 (O2A) conformer exhibiting a *syn* nucleobase orientation stabilized by an O2'H···O5' hydrogen-bonding interaction were found for all five protonated uridine nucleoside analogues, with TC more stable than the O2A for [Urd+H]+, [fl<sup>5</sup>Urd+H]+, and [cl<sup>5</sup>Urd+H]+ by 6.1, 3.4, and 3.8 kJ/mol and O2A favored over TC for [br<sup>5</sup>Urd+H]+ and [io<sup>5</sup>Urd+H]+ by 1.8 and 1.9 kJ/mol, respectively. Only gauche+ (293–303°) orientations of the 5'-hydroxy substituent were found among the low-energy conformers as this orientation is stabilized by a C6H···O5' noncanonical hydrogen-bonding interaction.

#### **DISCUSSION**

#### Conformations of [Urd+H]+ Populated by Electrospray Ionization

Combined IRMPD action spectroscopy and computational work has previously established that a diverse mixture of 2,4-dihydroxy tautomers and O4-protonated conformers of protonated

uridine are populated by electrospray ionization.<sup>24</sup> Among the 13 lowest-energy conformers, i.e., those examined in this work, spectral and energetic comparisons of the spectra predicted for these low-energy conformers to the measured IRMPD spectrum suggested that 10 conformers, Ti, TA, TB, TC, O4A, O4i, O4B, Tii, O4ii, and O4iii, may be among the experimentally accessed population. The calculated IR spectra of TA, TB, and Tii as well as O4A and O4i, and O4B and O4iii, respectively, are highly parallel. Least-squares fitting (LSF) found that TA, O4A, and O4B slightly better reproduce the measured spectrum than TB, O4i and O4iii. The best LSF of the measured spectrum was found for the Ti, TA, TC, O4A, O4B and O4ii conformers. The LSF results also indicated that the O2-protonated conformers, O2A and O2i, were not populated in the experiments. The various fits that gave rise to small residuals suggested that ~75% of the experimental population were T conformers and ~25% were O4 conformers.

#### Conformations of [fl<sup>5</sup>Urd+H]<sup>+</sup> Populated by Electrospray Ionization

The theoretical IR spectra predicted for the conformers of [fl<sup>5</sup>Urd+H]<sup>+</sup> that provide the best fits to the experimental IRMPD spectrum, i.e., **TB**, **Tii**, **O4i**, and **O4B**, are visually compared in Figure 6. Notably, the IR spectrum predicted for the ground **Ti** conformer is not included in this comparison as the feature predicted at 3515 cm<sup>-1</sup> is not observed and several of the features predicted in the fingerprint region are shifted relative to the measured IRMPD spectrum. The IR spectra predicted for the T and O4 (as well as the O2) conformers exhibit features in common as well as unique features or spectral shifting of features that are characteristic of the protonation site/tautomeric form. The best reproduction of the measured IRMPD spectrum is obtained from various combinations of T and O4 conformers. Similar comparisons for the **TA**, **O4A**, **Tiii**, and **O4ii** conformers that are or may also be populated in the experiments are shown in Figure S11. The predicted spectra for the **TA** and **O4A** conformers are very similar to those of the **TB** and **O4B** conformers and although their Gibbs energies are lower, the shapes of the spectral features of **TB** and **O4B** exhibit better agreement with the measured spectrum. Because the **O4A**, **Tiii**, and **O4ii** conformers lie 6.7–11.2 kJ/mol higher in relative Gibbs energy and do not exhibit unique spectral features that definitively demonstrate their presence in the experiments, they are likely

only minor contributors to the experimental population. Additional comparisons for low-energy conformers that exhibit spectral features or shifts in the band positions that preclude their presence in the experiments including the ground Ti conformer as well as the TC, O2i, O2A, and O4iii conformers, are given in Figure S12. The bands observed at ~1285, 1800, and 3390 cm<sup>-1</sup> in the measured IRMPD spectrum are not predicted for any of the T conformers, and thus establish the presence of O4-protonated conformers. The intensities of these bands are lower than predicted for all of the O4-protonated conformers indicating that they are present in lower abundance than the T conformers. Consistent with this interpretation, LSF of the IRMPD spectrum based on all 13 low-energy conformers provides the smallest residuals, but also predicts small features or shifting of features that are not consistent with the measured IRMPD spectrum (see Figure 13). Because the predicted spectra for the all of the low-energy conformers and in particular those having the same protonation site or tautomeric form exhibit similar spectra, and the LSF analysis does not bias against conformers with predicted features that are not observed, this single least-squares analysis is biased. Therefore, comprehensive least-squares analyses where all 2<sup>13</sup> possible combinations of the 13 low-energy conformers were performed. The discrepancies between the measured IRMPD and LSF spectra of [fl<sup>5</sup>Urd+H]<sup>+</sup> largely disappear when the Ti, TC, O2i, O2A, and O4iii conformers are excluded (see Figure S13). The various LSF that produce small residuals suggest that at least two T and two O4 conformers are needed to reproduce the measured spectrum and that the T conformers represent ~70–75% of the experimental population with the remainder 25–30% arising from O4 conformers.

#### Conformations of [cl<sup>5</sup>Urd+H]<sup>+</sup> Populated by Electrospray Ionization

The measured IRMPD spectrum of [cl<sup>5</sup>Urd+H]<sup>+</sup> is compared to the theoretical IR spectra predicted for the conformers that provide the best reproduction of the measured IRMPD spectrum, i.e., **O4i**, **O4B**, **TB**, and **Tii**, in Figure 7. As for [fl<sup>5</sup>Urd+H]<sup>+</sup>, the IR spectrum of the ground **Ti** conformer is again excluded from this comparison as several features exhibit shifts in the band positions relative to the measured spectrum that indicate that this conformer is not an important contributor. Not surprisingly, the IR spectra predicted for the T and O4 conformers are again

complementary such that combined they exhibit very good agreement with the measured IRMPD spectrum. However, we note that the features observed at ~ 3390 and 3490 cm<sup>-1</sup> are under and over predicted for all conformers, respectively. Additional comparisons for other conformers that are likely populated (at least in minor abundance) in the experiments, i.e., O4A, TA, O4ii, O4iii, and Tiii, are displayed in Figure S14. The predicted spectra for the O4A and O4B conformers, and likewise for the TA and TB conformers, are again very similar. Although the O4A and TA conformers are predicted to be more stable than the O4B and TB conformers, the shapes of the spectral features of the latter exhibit better agreement with the measured spectrum and suggest that contrary to energetic predictions, C3'-endo puckering is actually more favorable than C2'-endo. However, it is unclear whether this discrepancy arises due to differences in solution vs. gas phase stability or is a limitation of theory. Because the **O4ii**, **O4iii**, and **Tiii** conformers do not display any unique spectral features that confirm their presence in the experiments and further lie 4.5-10.1 kJ/mol higher in relative Gibbs energy, they are likely at best minor contributors to the experimental populations. Additional comparisons for low-energy conformers whose presence in the experiments is eliminated by spurious spectral features that are not experimentally observed or shifts in the band positions, i.e., the Ti, TC, O2i, and O2A conformers, are provided in Figure S15. The bands observed at ~1285, 1800, and 3390 cm<sup>-1</sup> in the measured IRMPD spectrum again establish the presence of O4-protonated conformers in the experiments. The intensities of these bands have increased relative to those in the spectrum of the [fl<sup>5</sup>Urd+H]<sup>+</sup> system, indicating that O4-protonated conformers comprise a larger portion of the experimental population, consistent with the relative Gibbs energies predicted for the T vs. O4 conformers of these systems (Table 1 and Figure 5). LSF of the IRMPD spectrum based on all 13 low-energy conformers again provides the smallest residuals, and again predicts addition features not observed and shifting of features that are not consistent with the measured IRMPD spectrum (see Figure S16). When the Ti, TC, O2i, and O2A conformers are excluded from the LSF, these differences disappear (see Figure S16). Consistent with the changes observed in the measured spectrum, spectral interpretation, and computed Gibbs energies, the various LSF that produce small residuals indicate that O4 conformers comprise a larger portion of the population, ~57–63%, with the remainder 37–43% arising from T conformers.

#### Conformations of [br5Urd+H]+ Populated by Electrospray Ionization

Given the high degree of similarity between the IRMPD spectra of [cl<sup>5</sup>Urd+H]<sup>+</sup> and [br<sup>5</sup>Urd+H]<sup>+</sup> (see Figure 2), it is not surprising that it is again the **O4i**, **O4B**, **Tii**, and **TB** conformers that best reproduce the measured IRMPD spectrum as shown in the comparisons of Figure 8. Similar comparisons for the ground O4A conformer as well as the O4ii, TA, O4iii, Tii, and Tiii conformers that are or may be populated in the experiments are provided in Figure S17. The four latter conformers lie 5.2–14.4 kJ/mol higher in relative Gibbs energy and lack spectral features that confirm their presence in the experiments, and therefore they are likely at best only minor contributors to the experimental population. Additional comparisons for low-energy conformers that exhibit spectral features or shifts in the band positions that are inconsistent with the measured spectrum eliminating their presence in the experiments, Ti, O2i, O2A, and TC, are given in Figure S18. The bands at ~1285, 1800, and 3395 cm<sup>-1</sup> in the measured spectrum once again confirm the presence of O4-protonated conformers in the experimental population. The relative intensities of these bands have again increased, indicating that O4-protonated conformers comprise a larger portion of the population, consistent with the relative Gibbs energies of the T vs. O4 conformers of these systems. LSF of the IRMPD spectrum based on all 13 low-energy conformers again exhibits spectral features and shifting of features that are not consistent with the measured IRMPD spectrum (see Figure S19). The differences between the spectra largely disappear when the Ti, O2i, O2A, and TC conformers are excluded (see Figure S19). Also consistent with the spectral interpretation and computed Gibbs energies, the various LSF that produce small residuals suggest that O4 conformers represent ~66-72% of the experimental population with the remainder 28–34% arising from T conformers.

#### Conformations of [io<sup>5</sup>Urd+H]<sup>+</sup> Populated by Electrospray Ionization

It is again the theoretical IR spectra predicted for the **O4i**, **O4B**, **TB**, and **Tii** conformers of [io<sup>5</sup>Urd+H]<sup>+</sup> that combined best reproduce the measured IRMPD spectrum; spectral

comparisons for these conformers are shown in Figure 9. Similar comparisons for other conformers that are or may be populated in the experiments, O4A, O4ii, TA, O4iii, and Tiii, are shown in Figure S20. Because the three latter conformer lies 6.5–14.3 kJ/mol higher in relative Gibbs energy and do not exhibit unique spectral features that confirm their presence in the experiments, they are likely minor contributors to the experiments. Additional comparisons for low-energy conformers exhibit spectral features or shifts in the band positions that are inconsistent with the measured spectrum, Ti, O2i, O2A, and TC, and thus are unlikely contributors in the experiments are given in Figure S21. The bands at ~1285, 1800, and 3395 cm<sup>-1</sup> in the measured spectrum once again confirm the presence of O4-protonated conformers in the experimental population. The relative intensities of these bands again indicate that O4-protonated conformers comprise a larger portion of the population than T conformers, consistent with the relative Gibbs energies predicted for the T vs. O4 conformers of these systems. LSF of the IRMPD spectrum based on all 13 low-energy conformers again predicts addition features not observed and shifting of features that are inconsistent with the measured IRMPD spectrum (see Figure S22). These disparities are largely removed when the Ti, O2i, O2A, and TC conformers are excluded (see Figure S22). Also consistent with the spectral interpretation, the various LSF that produce small residuals suggest that O4 conformers represent ~65–70% of the experimental population with the remainder 30–35% arising from T conformers, whereas the computed Gibbs energies suggest that O4 conformers represent >90% of the experimental population.

#### Conformations of [x<sup>5</sup>Urd+H]<sup>+</sup> Populated by Electrospray Ionization (ESI)

In summary, a diverse mixture of low-energy conformers of the protonated 5-halourdine nucleoside analogues are populated in the experiments. For all four  $[x^5\text{Urd+H}]^+$  analogues, 2,4-dihydroxy tautomers and O4-protonated conformers dominate the population, with O2-protonated conformers not populated in measurable abundance. The relative populations of the T vs. O4 conformers are sensitive to the 5-substituent of the nucleobase. Variations in the relative intensities of spectral features characteristic of the T and O4 conformers indicate that as for canonical  $[\text{Urd+H}]^+$ , T conformers dominate the experimental population for  $[\text{fl}^5\text{Urd+H}]^+$ . As the size of the

5-halogen substituent increases from F to Cl to Br to I, O4 conformers comprise an increasingly larger portion of the experimental population. The observed variation in the relative populations of T vs. O4 conformers is also consistent with the relative stabilities predicted for these species at the B3LYP/6-311+G(2d,2p) level of theory. Present results are consistent with previous findings for protonated uridine<sup>24</sup> and a series of sugar-modified uridine nucleoside analogues, ddUrd, dUrd, araUrd, Urdm, and Urdfl, where a diverse mixture of T and O4 conformers are populated. <sup>24,25,27,28</sup> Among these uridine nucleoside analogues, T conformers are favored over O4-protonated conformers for dUrd, Urd, Urdm, and Urdfl, whereas O4-protonated conformers are favored over T conformers for ddUrd and araUrd. In contrast, a diverse mixture of T and O2-protonated conformers are populated for the 5-methylated uridine nucleoside analogues, dThd, Thd, and Thdm. <sup>23,26</sup> For all three 5-methyluridine nucleoside analogues, T conformers are favored over O2. Clearly, the electron-withdrawing character of the 5-halogen substituents exerts a different influence on protonation preferences vs. the electron-donating 5-methyl substituent.

In the IRMPD spectra of all four [ $x^5$ Urd+H]<sup>+</sup> systems examined here, many of the spectral features exhibit asymmetry and broadening such that IRMPD spectra are best described by combinations of the IR spectra predicted for at least two low-energy T and two low-energy O4 conformers, with minor contributions from several additional T and O4 conformers. The dominant conformers populated for all four systems include **O4i**, **O4B**, **TB**, and **Tii** with relative abundances dependent on the 5-halogen substituent. Although the **O4A** and **TA** conformers are predicted to be more stable than **O4B** and **TB**, the shapes of the spectral features in the measured spectra suggest that they are somewhat less abundant indicating a preference for C3'-endo sugar puckering over C2'-endo among these conformers. The **O4i** conformer also exhibits C3'-endo sugar puckering, whereas **Tii** exhibits C2'-endo puckering. All four conformers exhibit *anti* nucleobase orientations stabilized by noncanonical C6H····O5' hydrogen-bonding interactions, which lead to gauche<sup>+</sup> orientations of the 5'-hydroxy substituents. Conformers with C2'-endo puckering also gain additional stabilization via noncanonical C2'H···O5' hydrogen-bonding interactions. No *syn* conformers are populated in the experiments. The most stable O4 conformers

also gain stabilization from interaction of the excess proton with the 5-halogen substituent, O4H<sup>+</sup>···X. This interaction produces red shifting in the O4–H<sup>+</sup> stretch. The magnitude of the red shifting is underpredicted by theory such that care must be taken in the interpretation of the IRMPD spectra. All of these conformers are additionally stabilized by either an O2′H···O3′ or O3′H···O2′ hydrogen-bonding interaction.

#### Resonant Vibrational Modes of [x<sup>5</sup>Urd+H]<sup>+</sup>

Vibrational assignments of the measured IRMPD spectral features for the [x<sup>5</sup>Urd+H]<sup>+</sup> systems are summarized in Table 2 and are based on the predicted IR spectra of the dominant conformations populated, the O4i, O4B, Tii, and TB conformers. In the IR fingerprint region, the bands observed at ~1800 cm<sup>-1</sup> arises from the free C=O2 carbonyl stretch of O4-protonated conformers; the frequency predicted for this stretch varies slightly depending on the sugar puckering and inductive effects of the 5-halogen substituent. Broadening and asymmetry in this spectral feature among all four IRMPD spectra indicate that multiple O4-protonated conformers are populated in the experiments. Likewise, the spectral feature observed at ~1245 or ~1275 cm<sup>-1</sup> also arises from O4-protonated conformers and is associated with a combination mode involving the O4-H<sup>+</sup> stretch. In the hydrogen-stretching region, the band observed at ~3395 cm<sup>-1</sup> is associated with N3-H stretching of O4-protonated conformers. The frequencies predicted for these latter stretches do not vary with the 5-halogen substituent, whereas their relative intensities vary markedly with the identity of the 5-substituent. Interestingly, the relative intensities of the spectral features are more indicative of the presence and importance of T conformers than the band positions, especially for [fl<sup>5</sup>Urd+H]<sup>+</sup>. However, as the size of the halogen substituent increases the bands observed at ~3575 and 3615 cm<sup>-1</sup> become characteristic of the T conformers and are associated with O2-H and O4-H stretching. All other major bands are contributed by both T and O4 conformers and thus are somewhat less diagnostic for differentiating such conformers, however many of the spectral features exhibit small shifts with changes in the local environment, i.e., nucleobase orientation, sugar puckering, and canonical and noncanonical hydrogen-bonding interactions that facilitate characterization of the conformer populations. Additional details of the vibrational mode assignments are summarized in Table 2.

#### Relative Glycosidic Bond Stabilities of [Urd+H]<sup>+</sup> and the [x<sup>5</sup>Urd+H]<sup>+</sup> Nucleosides Analogues

The survival yield curves measured for protonated uridine and the protonated 5-halouridine nucleoside analogues are compared in Figure 10. The CID<sub>50%</sub> values extracted from fits to these curves using eq 3 are also summarized in the figure and follow the order [Urd+H]<sup>+</sup> < [fl<sup>5</sup>Urd+H]<sup>+</sup> < [cl<sup>5</sup>Urd+H]<sup>+</sup> < [io<sup>5</sup>Urd+H]<sup>+</sup>. Regardless of the dissociation level compared, this trend is robust. Thus, the relative glycosidic bond stabilities of these species follow the same order because glycosidic bond cleavage via reaction 5 is the only dissociation pathway observed (and the number of degrees of freedom available to these systems is preserved across this series). This trend is also preserved when the experiments are performed under maximum resolution conditions ( $P_{He} = \sim 1$  mTorr in the ion trap) where the complementary glycosidic bond cleavage pathway of reaction 6 is observed as a minor dissociation pathway. Thus, the stability of the glycosidic bond is enhanced by 5-halogenation, and further the enhancement increases with the size of the halogen substituent.

The shapes of the survival yield curves provide additional insight into the relative glycosidic bond stabilities of these systems. The survival yield curves for [Urd+H]<sup>+</sup> and [fl<sup>5</sup>Urd+H]<sup>+</sup>, [br<sup>5</sup>Urd+H]<sup>+</sup>, and [io<sup>5</sup>Urd+H]<sup>+</sup> are very parallel with [fl<sup>5</sup>Urd+H]<sup>+</sup> exhibiting a mere 0.001 eV shift to higher rf<sub>EA</sub> values, whereas both [br<sup>5</sup>Urd+H]<sup>+</sup> and [io<sup>5</sup>Urd+H]<sup>+</sup> exhibit much larger shifts of ~0.041 and 0.045 eV, respectively. In contrast, the survival yield curve for [cl<sup>5</sup>Urd+H]<sup>+</sup> also exhibits a very small shift (increase to larger rf<sub>EA</sub>) relative to [fl<sup>5</sup>Urd+H]<sup>+</sup> near the onset for dissociation, but the survival yield falls off more slowly such that it is only slightly shifted (smaller rf<sub>EA</sub>) relative to [br<sup>5</sup>Urd+H]<sup>+</sup> and [io<sup>5</sup>Urd+H]<sup>+</sup> at rf<sub>EA</sub> values near complete dissociation. This behavior parallels the trend predicted for the relative stabilities of the T vs. O4 conformers across this series, and suggests that the glycosidic bond stability of the T conformers is lower than that of the O4 conformers, i.e., that tautomerization lowers the activation barrier(s) for N-glycosidic bond cleavage of the protonated uridine nucleoside analogues. Indeed, this same conclusion was drawn in earlier work where T conformers were found to predominantly influence

the threshold dissociation behavior of protonated uridine, and the absolute activation energy (AE) for glycosidic bond cleavage was determined using synergistic guided ion beam tandem mass spectrometry and theoretical approaches as  $113.9 \pm 3.9$  kJ/mol, in excellent agreement with the B3LYP/6-311+G(2d,2p) predicted values of 113.0 and 115.3 kJ/mol for T conformers.<sup>52</sup>

#### **Conclusions**

Synergistic IRMPD action spectroscopy, ER-CID experiments, and B3LYP/6-311+G(2d,2p)/B3LYP/6-311+G(d,p) theoretical calculations are employed in the present work to determine the influence of 5-halogenation on the structures and glycosidic bond stability of the protonated form of uridine. As found for protonated uridine, a diverse mixture of 2,4-dihydroxy tautomers and O4-protonated conformers are evident in the experimental populations of the protonated forms of the 5-halouridine nucleoside analogues accessed by electrospray ionization. The dominant contributors to the experimental populations include O4i, O4B, TB and Tii, with smaller contributions from O4A and TA, and minor contributions from O4ii, O4iii, and Tiii. Variations in the relative intensities of spectral features characteristic of the T vs. O4 conformers observed in the experimental IRMPD spectra indicate that their relative populations vary as a function of the 5-substituent. The T conformers dominate the population for canonical [Urd+H]<sup>+</sup> as well as that of [fl<sup>5</sup>Urd+H]<sup>+</sup>. However, as the size of the halogen substituent increases, O4 protonation become increasingly competitive such that O4 conformers dominate the populations for [cl<sup>5</sup>Urd+H]<sup>+</sup>, [br<sup>5</sup>Urd+H]<sup>+</sup> and [io<sup>5</sup>Urd+H]<sup>+</sup>. O2-protonated conformers do not measurably contribute to the experimental populations. Consistent with the absence of O2-protonated conformers in the experiments, theory predicts very little difference in the relative stabilities of O2 conformers as a function of the 5-substituent although 5-halogenation does very slightly stabilize these conformers. In all cases, multiple T and O4 conformers are found that lie lower in Gibbs energy that the most stable O2 conformer. The relative stabilities of the T vs. O4 conformers of these protonated uridine nucleoside analogues predicted at the B3LYP/6-311+G(2d,2p) are consistent with the spectral interpretations and the measured IRMPD spectra.

Survival yield analyses based on the ER-CID experiments suggest that 5-halogenation enhances the stability of the glycosidic bond, and that the enhancement increases with the size of the halogen substituent. The shapes of the survival yield curves suggest that the apparent enhancement in glycosidic bond stability as a function of the size of the halogen substituent may be largely driven by their influence on the relative stabilities (populations) of the T vs. O4 conformers. The shapes of these curves further suggest that the glycosidic bonds of the T conformers are weaker than those of the O4 conformers, i.e., that tautomerization lowers the activation barrier(s) for N-glycosidic bond cleavage of the protonated uridine nucleoside analogues consistent with conclusions drawn in earlier work where T conformers were found to predominantly influence the threshold dissociation behavior of protonated uridine.<sup>52</sup> In contrast to the present findings, 5-methylation alters the preferences of O2- vs. O4-protonation such that mixtures of T and O2 conformers are populated by electrospray ionization. Thus, both nucleobase and sugar modifications of uridine nucleoside analogues provide effective means by which the relative populations of various 2,4-dihydroxy, and O4- and O2 protonated structures can be manipulated and further alter glycosidic bond stability.

#### ASSOCIATED CONTENT

#### **Supporting Information**

The Supporting Information is available free of charge at <a href="https://pubs/acs.org/doi/10.1021/jasms.\*\*\*">https://pubs/acs.org/doi/10.1021/jasms.\*\*\*</a>

Figures comparing the stable low-energy B3LYP/6-311+G(d,p) conformations of the neutral and protonated forms of the  $x^5$ Urd nucleoside analogues and their B3LYP/6-311+G(2d,2p) relative Gibbs energies at 298 K; comparisons of the experimental IRMPD action spectra of  $[x^5$ Urd+H]<sup>+</sup> with the B3LYP/6-311+G(d,p) optimized structures and calculated linear IR spectra predicted for stable low-energy conformations that are minor contributors and those not experimentally populated (PDF).

#### **AUTHOR INFORMATION**

#### **Corresponding Author**

Mary T. Rodgers - Department of Chemistry, Wayne State University, Detroit, Michigan, 48202, United States; orcid.org/0000-0002-5614-0948; Phone (313) 577-2431; Email: mrodgers@chem.wayne.edu

#### **Authors**

**Neven N. Mikawy** - Department of Chemistry, Wayne State University, Detroit, Michigan, 48202, United States; orcid.org/0000-0001-8639-5995

**Harrison A. Roy** - Department of Chemistry, Wayne State University, Detroit, Michigan, 48202, United States; orcid.org/0000-0002-9128-5245

**Ezekiel Israel** - Department of Chemistry, Wayne State University, Detroit, Michigan, 48202, United States; orcid.org/0000-0002-5563-9720

**Lucas A. Hamlow** - Department of Chemistry, Wayne State University, Detroit, Michigan, 48202, United States; orcid.org/0000-0002-7988-5117

**Yanlong Zhu** - Department of Chemistry, Wayne State University, Detroit, Michigan, 48202, United States; orcid.org/0000-0003-4909-7336

**Giel Berden** – *Radboud University, Institute for Molecules and Materials, FELIX Laboratory, Nijmegen, The Netherlands;* orcid.org/0000-0003-1500-922X

**Jos Oomens** – Radboud University, Institute for Molecules and Materials, FELIX Laboratory, Nijmegen, The Netherlands; orcid.org/0000-0002-2717-1278

**Clifford E. Frieler -** Department of Chemistry, Wayne State University, Detroit, Michigan, 48202, United States

#### **ACKNOWLEDGMENTS**

This work was financially supported by the National Science Foundation, under Grants OISE-1357787 (for international travel expenses), DBI-0922819 (for the Bruker amaZon ETD QITMS employed in this work), and CHE-1709789 (for other research costs). The authors acknowledge support from the Egyptian Ministry of Science for N.N.M, and from Wayne State University Summer Dissertation Fellowships for H.A.R, L.A.H, Y.Z and Thomas C. Rumble Graduate Research Fellowships for L.A.H and Y.Z. We also thank Wayne State University C&IT for excellent computational resources and support , and the Nederlandse Organisatie voor Wetenschappelijk Onderzoek (NWO) for the support of the FELIX Laboratory. The skillful assistance of the FELIX staff is gratefully acknowledged.

#### REFERENCES

- 1. Chatterjee, N.; Walker, G. C. Mechanisms of DNA Damage, Repair, and Mutagenesis. *Environ. Mol. Mutagen.* **2017**, *58*, 235–263.
- 2. Antoniali, G.; Malfatti, M. C.; Tell, G. Unveiling the Non-repair Face of the Base Excision Repair Pathway in RNA Processing: A Missing Link between DNA Repair and Gene Expression? *DNA Repair* **2017**, *56*, 65–74.
- 3. Vohhodina, J.; Harkin, D. P.; Savage, K. I. Dual Roles of DNA Repair Enzymes in RNA Biology/Post-transcriptional Control. *Wiley Interdiscip. Rev. RNA* **2016**, *7*, 604–619.
- 4. Wallace, S. S. Base Excision Repair: A Critical Player in Many Games. *DNA Repair* **2014**, *19*, 14–26.
- 5. Tsutakawa, S. E.; Lafrance-Vanasse, J.; Tainer, J. A. The Cutting Edges in DNA Repair, Licensing, and Fidelity: DNA and RNA Repair Nucleases Sculpt DNA to Measure Twice, Cut Once. *DNA Repair* **2014**, *19*, 95–107.
- 6. Drohat, A. C.; Maiti, A. Mechanisms for Enzymatic Cleavage of the N-Glycosidic Bond in DNA. *Org. Biomol. Chem.* **2014**, *12*, 8367–8378.
- 7. Bennett, M. T.; Rodgers, M. T.; Hebert, A. S.; Ruslander, L. E.; Eisele, L.; Drohat, A. C. Specificity of Human Thymine DNA Glycosylase Depends on N-Glycosidic Bond Stability. *J. Am. Chem. Soc.* **2006**, *128*, 12510–12519.
- 8. Boehmer, P. E.; Lehman, I. R. Herpes Simplex Virus DNA Replication. *Annu. Rev. Biochem.* **1997**, *66*, 347–384.
- 9.Pietro, B.; Filip, S.; Angana, R.; Andrea, C.; Sunandan, M.; Elżbieta, P.; Małgorzata, K.; Niloofar, S.; Eliana, D.; Paula, G.; Gülben, A.; Antonia, R.; Pınar, P.; Erik, D.; Silvestro, G. C.; Francesca, A.; Janusz, M. B. A Database of RNA Modification Pathways. *Nucleic Acids Res.* 2022, 50, D231–D235.
- 10. Mathe, C.; Gosselin, G. L-Nucleoside Enantiomers as Antiviral Drugs: A Mini-Review. *Antiviral Res.* **2006**, *71*, 276–281.
- 11. Alberti, A.; Caporaso, N. HBV Therapy: Guidelines and Open Issues. *Dig. Liver Dis.* **2011**, *43S*, S57–S63.
- 12. Buster, E. H.; van Erpecum, K. J.; Schalm, S. W.; Zaaijer, H. L.; Brouwer, J. T.; Gelderblom, H. C.; de Knegt, R. J.; Minke Bakker, C.; Reesink, H. W.; Janssen, H. L. Treatment of Chronic Hepatitis B Virus Infection Dutch National Guidelines. *Neth. J. Med.* **2008**, *66*, 292–306.
- 13. Liaw, Y. F.; Natural History of Chronic Hepatitis B Virus Infection and Long-term Outcome Under Treatment. *Liver Int.* **2009**, *29*, 100–107.
- 14. Clercq, E. D. The Design of Drugs for HIV and HCV. Nat. Rev. Drug Discov. 2007, 6, 1001.
- 15. Clercq, E. D. Anti-HIV Drugs: 25 Compounds Approved within 25 Years After the Discovery of HIV. *Int. J. Antimicrob. Agents* **2009**, *33*, 307–320.
- 16. Biron, K. K. Antiviral Drugs for Cytomegalovirus Diseases. *Antiviral Res.* **2006**, *71*, 154–163.
- 17. Zhang, J.; Visser, F.; King, K. M.; Baldwin, S. A.; Young, J. D.; Cass, C. E. The Role of Nucleoside Transporters in Cancer Chemotherapy with Nucleoside Drugs. *Cancer Metastasis Rev.* **2007**, *26*, 85–110.
- 18. Wolken, J. K.; Turecek, F. P. Proton Affinity of Uracil. A Computational Study of Protonation Sites. *J. Am. Soc. Mass Spectrom.* **2000**, *11*, 1065-1071.

- 19. Kryachko, E. S.; Nguyen, M. T.; Zeegers-Huyskens, T. Theoretical Study of Tautomeric Forms of Uracil. 1. Relative Order of Stabilities and Their Relation to Proton Affinities and Deprotonation Enthalpies. *J. Phys. Chem. A* **2001**, *105*, 1288-1295.
- 20. Salpin, J. Y.; Guillaumont, S.; Tortajada, J.; MacAleese, L.; Lemaire, J.; Maitre, P. Infrared Spectra of Protonated Uracil, Thymine and Cytosine. *Chem Phys Chem* **2007**, *8*, 2235-44.
- 21. Nei, Y. w.; Akinyemi, T. E.; Steill, J. D.; Oomens, J.; Rodgers, M. T. Infrared Multiple Photon Dissociation Action Spectroscopy of Protonated Uracil and Thiouracils: Effects of Thioketo-Substitution on Gas-Phase Conformation. *Int. J. Mass Spectrom.* **2010**, *297*, 139-151.
- 22. Crampton, K. T.; Rather, A. I.; Nei, Y.-w.; Berden, G.; Oomens, J.; Rodgers, M. T. Protonation Preferentially Stabilizes Minor Tautomers of the Halouracils: IRMPD Action Spectroscopy and Theoretical Studies. *J. Am. Soc. Mass Spectrom.* **2012**, *23*, 1469-78.
- 23. Wu, R. R.; Yang, B.; Frieler, C. E.; Berden, G.; Oomens, J.; Rodgers, M. T. 2,4-Dihydroxy and O2 Protonated Tautomers of dThd and Thd Coexist in the Gas Phase: Methylation Alters Protonation Preferences versus dUrd and Urd. J. Am. Soc. Mass Spectrom. 2016, 27, 410-421.
- 24. Wu, R. R.; Yang, B.; Frieler, C. E.; Berden, G.; Oomens, J.; Rodgers, M. T. Diverse Mixtures of 2,4-Dihydroxy Tautomers and O4 Protonated Conformers of Uridine and 2'-Deoxyuridine Coexist in the Gas Phase. *Phys. Chem. Chem. Phys.* **2015**, *17*, 25978-25988.
- 25. Hamlow, L. A.; Devereaux, Z. J.; Roy, H. A.; Cunningham, N. A.; Berden, G.; Oomens, J.; Rodgers, M. T. Impact of the 2' and 3'-Sugar Hydroxyl Moieties on Gas-Phase Nucleoside Structure. *J. Am. Soc. Mass Spectrom.* **2019**, *30*, 832-845.
- 26. He, C. C.; Hamlow, L. A.; Zhu, Y.; Nei, Y. w.; Fan, L.; McNary, C. P.; Maître, P.; Steinmetz, V.; Schindler, B.; Compagnon, I.; Armentrout, P. B.; Rodgers, M. T. Structural and Energetic Effects of O2'-Ribose Methylation of Protonated Pyrimidine Nucleosides. *J. Am. Soc. Mass Spectrom.* **2019**, *30*, 2318-2334.
- 27. Devereaux, Z. J.; Roy, H. A.; He, C. C.; Zhu, Y.; Cunningham, N. A.; Hamlow, L. A.; Berden, G.; Oomens, J.; Rodgers, M. T. Influence of 2'-Fluoro Modification on Glycosidic Bond Stabilities and Gas-Phase Ion Structures of Protonated Pyrimidine Nucleosides. *J. Fluorine Chem.* 2019, 219, 10–22.
- 28. Hamlow, L. A.; He, C. C.; Devereaux, Z. J.; Roy, H. A.; Cunningham, N. A.; Soley, E. O.; Berden, G.; Oomens, J.; Rodgers, M. T. Gas-Phase Structures of Protonated Arabino Nucleosides. *Int. J. Mass Spectrom.* **2019**, *438*, 124-134.
- 29. Asakura, J.; Robins, M. J. Cerium (IV)-Mediated Halogenation at C-5 of Uracil Derivatives. *J. Org. Chem.* **1990**, *55*, 4928-4933.
- 30. Kumar, R.; Wiebe, L. I.; Knaus, E. E. A Mild and Efficient Methodology for the Synthesis of 5-Halogeno Uracil Nucleosides that Occurs via a 5-Halogeno-6-azido-5,6-dihydro intermediate. *Can. J. Chem.* **1994**, 72.
- 31. Aerschot, A.V.; Everaert, D.; Balzarini, J.; Augustyns, K.; Jie, L.; Janssen, G.; Peeters, O.; Blaton, H.; De Ranter, C.; De Clercq, E.; Herdewijn, P. Synthesis and Anti-HIV Evaluation of 2',3'-Dideoxyribo-5-chloropyrimidine Analogues: Reduced Toxicity of 5-Chlorinated 2',3'-Dideoxynucleosides. *J. Med. Chem.* **1990**, *33*, 1833.
- 32. Mercer, J. R.; Xu, L. H.; Knaus, E. E.; Wiebe, L. I. Synthesis and Tumor Uptake of 5-82Br-and 5-131I-Labeled 5-Halo-1–(2-fluoro-2-deoxy-beta-D-ribofuranosyl) Uracils. *J. Med. Chem.* **1989**, *32*, 1289.
- 33. Valle, J. J.; Eyler, J. R.; Oomens, J.; Moore, D. T.; van der Meer, A. F. G.; von Helden, G.; Meijer, G.; Hendrickson, C. L.; Marshall, A. G.; Blakney, G. T. Free Electron Laser-Fourier

- Transform Ion Cyclotron Resonance Mass Spectrometry Facility for Obtaining Infrared Multiphoton Dissociation Spectra of Gaseous Ions. *Rev. Sci. Instrum.* **2005**, *76*, 023103.
- 34. Polfer, N. C.; Oomens, J.; Moore, D. T.; von Helden, G.; Meijer, G.; Dunbar, R. C. Infrared Spectroscopy of Phenylalanine Ag(I) and Zn(II) Complexes in the Gas Phase. *J. Am. Chem. Soc.* **2006**, *128*, 517-525.
- 35. Polfer, N. C.; Oomens, J. Reaction Products in Mass Spectrometry Elucidated with Infrared Spectroscopy. *Phys. Chem. Chem. Phys.* **2007**, *9*, 3804-17.
- 36. Oepts, D.; van der Meer, A. F. G.; van Amersfoort, P. W. The Free-Electron-Laser User Facility FELIX. *Infrared Phys. Technol.* **1995**, *36*, 297-308.
- 37. Memboeuf, A.; Nasioudis, A.; Indelicato, S.; Pollreisz, F.; Kuki, A.; Keki, S.; van den Brink, O. F.; Vekey, K.; Drahos, L. Size Effect on Fragmentation in Tandem Mass Spectrometry. *Anal. Chem.* **2010**, *82*, 2294-302.
- 38. Derwa, F.; Depauw, E.; Natalis, P. New Basis for a Method for the Estimation of Secondary Ion Internal Energy Distributions in 'Soft' Ionization Techniques. *Org. Mass Spectrom.* **1991**, *26*, 117-118.
- 39. Guo, X. H.; Duursma, M. C.; Kistemaker, P. G.; Nibbering, N. M. M.; Vekey, K.; Drahos, L.; Heeren, R. M. A. Manipulating Internal Energy of Protonated Biomolecules in Electrospray Ionization Fourier Transform Ion Cyclotron Resonance Mass Spectrometry. *J. Mass Spectrom.* **2003**, *38*, 597-606.
- 40. Memboeuf, A.; Jullien, L.; Lartia, R.; Brasme, B.; Gimbert, Y. Tandem Mass Spectrometric Analysis of a Mixture of Isobars Using the Survival Yield Technique. *J. Am. Soc. Mass Spectrom.* **2011**, *22*, 1744-1752.
- 41. Zhu, Y.; Hamlow, L. A.; He, C. C.; Lee, J. K.; Gao, J.; Berden, G.; Oomens, J.; Rodgers, M.T. Gas-Phase Conformations and N-Glycosidic Bond Stabilities of Sodium Cationized 2'-Deoxyguanosine and Guanosine: Sodium Cations Preferentially Bind to the Guanine Residue. *J. Phys. Chem. B* **2017**, *121*, 4048–4060.
- 42. Zhu, Y.; Hamlow, L. A.; He, C. C.; Strobehn, S. F.; Lee, J. K.; Gao, J.; Berden, G.; Oomens, J.; Rodgers, M. T. Influence of Sodium Cationization versus Protonation on the Gas-Phase Conformations and Glycosidic Bond Stabilities of 2'-Deoxyadenosine and Adenosine. *J. Phys. Chem.* B **2016**, *120*, 8892–8904.
- 43. Zhu, Y.; Roy, H. A.; Cunningham, N. A.; Strobehn, S. F.; Gao, J.; Munshi, M. U.; Berden, G.; Oomens, J.; Rodgers, M. T. IRMPD Action Spectroscopy, ER-CID Experiments, and Theoretical Studies of Sodium Cationized Thymidine and 5-Methyluridine: Kinetic Trapping During the ESI Desolvation Process Preserves the Solution Structure of [Thd+Na]<sup>+</sup>. *J. Am. Soc. Mass Spectrom.* **2017**, *28*, 2423–2437.
- 44. Zhu, Y.; Roy, H. A.; Cunningham, N. A.; Strobehn, S. F.; Gao, J.; Munshi, M. U.; Berden, G.; Oomens, J.; Rodgers, M. T. Effects of Sodium Cationization versus Protonation on the Conformations and N-Glycosidic Bond Stabilities of Sodium Cationized Urd and dUrd: Solution Conformation of [Urd+Na]<sup>+</sup> is Preserved upon ESI. *Phys. Chem. Chem. Phys.* **2017**, *19*, 17637–17652.
- 45. Zhu, Y.; Hamlow, L. A.; He, C. C.; Roy, H. A.; Cunningham, N. A.; Munshi, M.; Berden, G.; Oomens, J.; Rodgers, M. T. Conformations and N-Glycosidic Bond Stabilities of Sodium Cationized 2'-Deoxycytidine and Cytidine: Solution Conformation of [Cyd+Na]<sup>+</sup> is Preserved upon ESI. *Int. J. Mass Spectrom.* **2018**, *429*, 18–27.
- 46. He, C. C.; Hamlow, L. A.; Devereaux, Z. J.; Zhu, Y.; Nei, Y.-w.; Fan, L.; McNary, C. P.; Maître, P.; Steinmetz, V.; Schindler, B.; Compagnon, I.; Armentrout, P. B.; Rodgers, M. T.

- Structural and Energetic Effects of 2'-Ribose Methylation of Protonated Purine Nucleosides. J. Phys. Chem. B 2018, 122, 9147–9160.
- 47. Devereaux, Z. J.; Zhu, Y.; Rodgers, M. T. Relative Glycosidic Bond Stabilities of Naturally-Occurring Methylguanosines: 7-Methylation is Intrinsically Activating. *Eur. J. Mass Spectrom.* **2019**, *25*, 16–29.
- 48. Kertesz, T. M.; Hall, L. H.; Hill, D. W.; Grant, D. F. CE50: Quantifying Collision Induced Dissociation Energy for Small Molecule Characterization and Identification. *J. Am. Soc. Mass Spectrom.* **2009**, *20*, 1759-1767.
- 49. HyperChem Computational Chemistry Software Package, Version 5.0, Hypercube, Inc., Gainsville, FL, 1997.
- Frisch, M. J.; Trucks, G. W.; Schlegel, H. B.; Scuseria, G. E.; Robb, M. A.; Cheeseman, J. R.; Scalmani, G.; Barone, V.; Mennucci, B.; Petersson, G. A., Nakatsuji, H., Caricato, M., Li, X., Hratchian, H. P., Izmaylov, A. F., Bloino, J., Zheng, G., Sonnenberg, J. L., Hada, M., Ehara, M., Toyota, K., Fukuda, R., Hasegawa, J., Ishida, M., Nakajima, T., Honda, Y., Kitao, O., Nakai, H., Vreven, T., Montgomery, Jr. J. A., Peralta, J. E., Ogliaro, F., Bearpark, M., Heyd, J. J., Brothers, E., Kudin, K. N., Staroverov, V. N., Kobayashi, R., Normand, J., Raghavachari, K., Rendell, A., Burant, J. C., Iyengar, S. S., Tomasi, J., Cossi, M., Rega, N., Millam, J. M., Klene, M., Knox, J. E., Cross, J. B., Bakken, V., Adamo, C., Jaramillo, J., Gomperts, R., Stratmann, R. E., Yazyev, O., Austin, A. J., Cammi, R., Pomelli, C., Ochterski, J. W., Martin, R. L., Morokuma, K., Zakrzewski, V. G., Voth, G. A., Salvador, P., Dannenberg, J. J., Dapprich, S., Daniels, A. D., Farkas, O", Foresman, J. B., Ortiz, J. V., Cioslowski, J., Fox, D. J. Gaussian 16, Revision C.01, Gaussian, Inc., Wallingford, CT, 2016.
- 51. Oomens, J.; Tielens, A. G. G. M.; Sartakov, B.; von Helden, G.; Meijer, G. Laboratory Infrared Spectroscopy of Cationic Polycyclic Aromatic Hydrocarbon Molecules. *Astrophys. J.* **2003**, *591*, 968-985.
- 52. Wu, R. R.; Rodgers, M. T. Tautomerization Lowers the Activation Barriers for Glycosidic Bond Cleavage of Protonated Uridine and 2'-Deoxyuridine. *Phys. Chem. Chem. Phys.* **2016**, *18*, 24451-24459.

**Table 1.** Relative Enthalpies and Gibbs Energies of Select Stable Low-Energy Conformers of the Protonated Forms of Uridine and the 5-Halouridine Nucleoside Analogues at 0 and 298 K in kJ/mol<sup>a</sup>

Species	Conformer	$\Delta H_0$	$\Delta H_{298}$	$\Delta G_{298}$
[Urd+H] <sup>+b</sup>	Ti	0.0	0.0	0.0
	TA	1.0	2.2	0.2
	TB	3.4	4.6	2.5
	TC	2.1	2.3	2.9
	O4A	4.6	6.3	2.9
	O4i	3.5	5.0	3.0
	O4B	5.6	7.2	4.4
	Tii	6.0	7.2	5.5
	O4ii	7.0	8.1	6.4
	O2i	8.6	8.9	8.0
	Tiii	8.6	10.0	8.1
	O2A	8.5	8.8	9.0
	O4iii	10.7	12.0	9.6
[fl <sup>5</sup> Urd+H] <sup>+</sup>	Ti	0.0	0.0	0.0
[]	TA	1.7	2.8	1.1
	TB	4.2	5.3	3.4
	TC	4.4	4.5	5.3
	O2i	6.5	6.6	6.4
	Tii	6.9	7.9	6.5
	O4A	7.9	9.4	6.7
	O4i	7.1	8.5	6.8
	O4B	8.8	10.3	7.8
	O2A	8.2	8.4	8.7
	Tiii	9.7	11.1	9.2
	O4ii	11.4	12.3	11.2
	O4iii	14.1	15.5	13.2
[cl <sup>5</sup> Urd+H] <sup>+</sup>	Ti	0.0	0.0	0.0
	O4A	1.8	3.3	0.4
	O4i	1.2	2.6	0.8
	TA	1.9	3.1	1.1
	O4B	2.8	4.3	1.8
	TB	4.6	5.8	3.6
	TC	3.7	3.7	4.4
	O4ii	4.5	5.4	4.5
	O2i	6.8	6.9	6.1
	Tii	7.2	8.2	7.0
	O4iii	7.9	9.3	7.1
	O2A	7.7	7.9	8.2
	Tiii	10.5	11.7	10.1

**Table 1.** (continued) Relative Enthalpies and Gibbs Energies of Select Stable Low-Energy Conformers of the Protonated Forms of Uridine and the 5-Halouridine Nucleoside Analogues at 0 and 298 K in kJ/mol<sup>a</sup>

Species	Conformer	$\Delta H_0$	$\Delta H_{298}$	$\Delta G_{298}$
[br <sup>5</sup> Urd+H] <sup>+</sup>	O4A	0.9	1.1	0.0
	O4i	0.0	0.0	0.5
	O4B	2.7	2.8	2.7
	O4ii	2.8	2.3	3.1
	Ti	4.6	3.4	4.9
	TA	5.5	5.4	5.2
	O2i	5.8	4.6	6.2
	O4iii	7.4	7.7	6.6
	O2A	6.6	5.6	7.8
	TB	8.8	8.7	9.0
	TC	8.1	6.9	9.6
	Tii	11.0	11.0	10.7
	Tiii	13.8	13.9	14.4
[io <sup>5</sup> Urd+H] <sup>+</sup>	O4i	0.0	0.0	0.0
	O4A	1.4	1.6	0.6
	O4ii	2.5	2.1	2.3
	O4B	2.9	3.0	2.4
	Ti	5.8	4.5	6.4
	TA	6.7	6.6	6.5
	O2i	6.6	5.5	7.0
	O4iii	7.9	8.0	7.7
	O2A	7.1	6.1	8.6
	TB	9.8	9.7	9.1
	TC	8.7	7.4	10.5
	Tii	12.3	12.1	12.8
	Tiii	14.5	14.7	14.3

<sup>&</sup>lt;sup>a</sup>Energetics based calculations performed at the B3LYP/6-311+G(2d,2p) level of theory, including ZPE and thermal corrections based on the B3LYP/6-311+G(d,p) optimized structures and vibrational frequencies. <sup>b</sup>Results for [Urd+H]<sup>+</sup> taken from ref 24.

**Table 2.** Vibrational Mode Assignments for  $[Urd+H]^+$  and  $[x^5Urd+H]^{+a}$ 

Vibrational Mode	[Urd+H] <sup>+b</sup>	[fl <sup>5</sup> Urd+H] <sup>+</sup>	[cl <sup>5</sup> Urd+H] <sup>+</sup>	[br <sup>5</sup> Urd+H] <sup>+</sup>	[io <sup>5</sup> Urd+H] <sup>+</sup>
Sugar and nucleobase ring	-	766	760	760	765
Sugar ring stretching with C4′–H and C5′–H bending	-	910	870	865	880
C1'-H, C2'-H, and O2'-H bending	-	1075	1080	-	1065
Sugar ring stretching	1115 <sup>b</sup>	1110	1119	1105	1100
Sugar ring stretching with O2'–H bending	-	1140	-	1145	-
O2–H or O4–H and C2′–H stretching	1210 <sup>b</sup>	1195	1204	1201	1200
O4–H, N1–C2, C1′–H, C2′–H stretching	1245	1245	1273	1271	1276
C2'-H, C3'-H, and O3'-H bending	1380	1376	1404	1406	1406
Nucleobase ring stretching with C5–H, C5–X, and C6–H bending	1505 <sup>b</sup>	1525	1510	1510	1515
C4–C5 stretching with O4–H bending; N1–C2 stretching with O2–H bending	1595 <sup>b</sup>	1614	1583	1574	1561
C2-N3 and C5=C6 stretching	1650 <sup>b</sup>	1653	1627	1614	1609
C2=O stretching	1800 <sup>b</sup>	1799	1793	1794	1799
N3-H stretching	3395 b	3389	3397	3393	3389
O4–H and/or O2–H stretching with O2′–H bending	3510 <sup>b</sup>		3493	3461	3417
O2–H, O4–H, O2′–H, O3′–H stretching	3565 b	3557, 3577	3557, 3573	3557, 3573	3553, 3573
O4-H and O2'-H stretching	3615 <sup>b</sup>	3617	3609	3613	3609
O2'-H, O3'-H, and O5'-H stretching	3665 b	3661	3660	3665	3657

<sup>&</sup>lt;sup>a</sup>All values are given in cm<sup>-1</sup>. <sup>b</sup>Results for [Urd+H]<sup>+</sup> are taken from ref 24.

#### **Figure Captions**

**Figure 1.** Chemical structures of uridine (Urd), 5-fluorouridine (fl<sup>5</sup>Urd), 5-chlorouridine (cl<sup>5</sup>Urd), 5-bromouridine (br<sup>5</sup>Urd), and 5-iodouridine (io<sup>5</sup>Urd). The numbering of the nucleobase and sugar moieties are shown.

**Figure 2.** Infrared multiple photon dissociation (IRMPD) action spectra of the protonated forms of uridine,  $[Urd+H]^+$ , and the 5-halouridines,  $[x^5Urd+H]^+$ , where  $xUrd = fl^5Urd$ ,  $cl^5Urd$ ,  $br^5Urd$ , and io  $^5Urd$ , in the IR fingerprint and hydrogen-stretching regions. Data for  $[Urd+H]^+$  was taken from ref 24.

**Figure 3.** CID mass spectra of the protonated forms of uridine,  $[Urd+H]^+$ , and the 5-halouridines,  $[x^5Urd+H]^+$ , where  $xUrd = fl^5Urd$ ,  $cl^5Urd$ ,  $br^5Urd$ , and  $io^5Urd$ . The spectra shown were acquired at an rf excitation amplitude ( $rf_{EA}$ ) that produces ~50% dissociation of the precursor ion.

**Figure 4.** Pseudorotation phase angles (*P*), glycosidic bond angles, and 5'-hydroxy orientations of the ground and low-energy conformers of uridine, Urd, the 5-halouridines,  $x^5$ Urd, the protonated forms of uridine,  $[\text{Urd+H}]^+$ , and the protonated forms of the 5-halouridines,  $[x^5\text{Urd+H}]^+$ , where  $x\text{Urd} = \text{fl}^5\text{Urd}$ ,  $\text{cl}^5\text{Urd}$ ,  $\text{br}^5\text{Urd}$ , and  $\text{io}^5\text{Urd}$ .

**Figure 5.** B3LYP/6-311+G(2d,2p) relative Gibbs energies at 298 K of the 13 most stable lowenergy conformers of protonated uridine,  $[Urd+H]^+$ , and the protonated 5-halouridines,  $[x^5Urd+H]^+$ , where  $xUrd = fl^5Urd$ ,  $cl^5Urd$ ,  $br^5Urd$ , and  $io^5Urd$ . Values are also summarized in Table 1. The T, O4, and O2 conformers are color-coded and offset to facilitate comparisons and visualization of the trends as function of the 5-substituent.

**Figure 6.** Comparison of the experimental IRMPD action spectrum of [fl<sup>5</sup>Urd+H]<sup>+</sup> with the B3LYP/6-311+G(d,p) optimized structures and calculated linear IR spectra for representative low-energy conformers, **TB**, **Tii**, **O4i**, and **O4B**, that combined provide the best match to the measured spectrum. The nucleobase orientation, sugar puckering, and B3LYP/6-311+G(2d,2p) relative Gibbs energies at 298 K are also shown. The measured IRMPD spectrum is overlaid with each theoretical spectrum and scaled to match the intensity of the most intense computed band in both the IR fingerprint and hydrogen-stretching regions to facilitate comparisons.

**Figure 7.** Comparison of the experimental IRMPD action spectrum of [cl<sup>5</sup>Urd+H]<sup>+</sup> with the B3LYP/6-311+G(d,p) optimized structures and calculated linear IR spectra for representative low-energy conformers, **O4i**, **O4B**, **TB**, and **Tii**, that combined provide the best match to the measured spectrum. The nucleobase orientation, sugar puckering, and B3LYP/6-311+G(2d,2p) relative Gibbs energies at 298 K are also shown. The measured IRMPD spectrum is overlaid with each theoretical spectrum and scaled to match the intensity of the most intense computed band in both the IR fingerprint and hydrogen-stretching regions to facilitate comparisons.

**Figure 8.** Comparison of the experimental IRMPD action spectrum of [br<sup>5</sup>Urd+H]<sup>+</sup> with the B3LYP/6-311+G(d,p) optimized structures and calculated linear IR spectra for representative low-energy conformers, **O4i**, **O4B**, **TB**, and **Tii** that combined provide the best match to the measured spectrum. The nucleobase orientation, sugar puckering, and B3LYP/6-311+G(2d,2p) relative Gibbs energies at 298 K are also shown. The measured IRMPD spectrum is overlaid with each theoretical spectrum and scaled to match the intensity of the most intense computed band in both the IR fingerprint and hydrogen-stretching regions to facilitate comparisons.

**Figure 9.** Comparison of the experimental IRMPD action spectrum of [io<sup>5</sup>Urd+H]<sup>+</sup> with the B3LYP/6-311+G(d,p) optimized structures and calculated linear IR spectra for representative low-energy conformers, **O4i**, **O4B**, **TB**, and **Tii**, that combined provide the best match the measured spectrum. The nucleobase orientation, sugar puckering, and B3LYP/6-311+G(2d,2p) relative Gibbs energies at 298 K are also shown. The measured IRMPD spectrum is overlaid with each theoretical spectrum and scaled to match the intensity of the most intense computed band in both the IR fingerprint and hydrogen-stretching regions to facilitate comparisons.

**Figure 10.** Survival yield curves of the protonated forms of uridine,  $[Urd+H]^+$ , and the 5-halouridines,  $[x^5Urd+H]^+$ , where  $xUrd = fl^5Urd$ ,  $cl^5Urd$ ,  $br^5Urd$ , and  $io^5Urd$ . Fits to the survival yield curves and  $CID_{50\%}$  values extracted from four-parameter logistic fits to the survival yield curves are also shown.

Figure 1.

Figure 2.

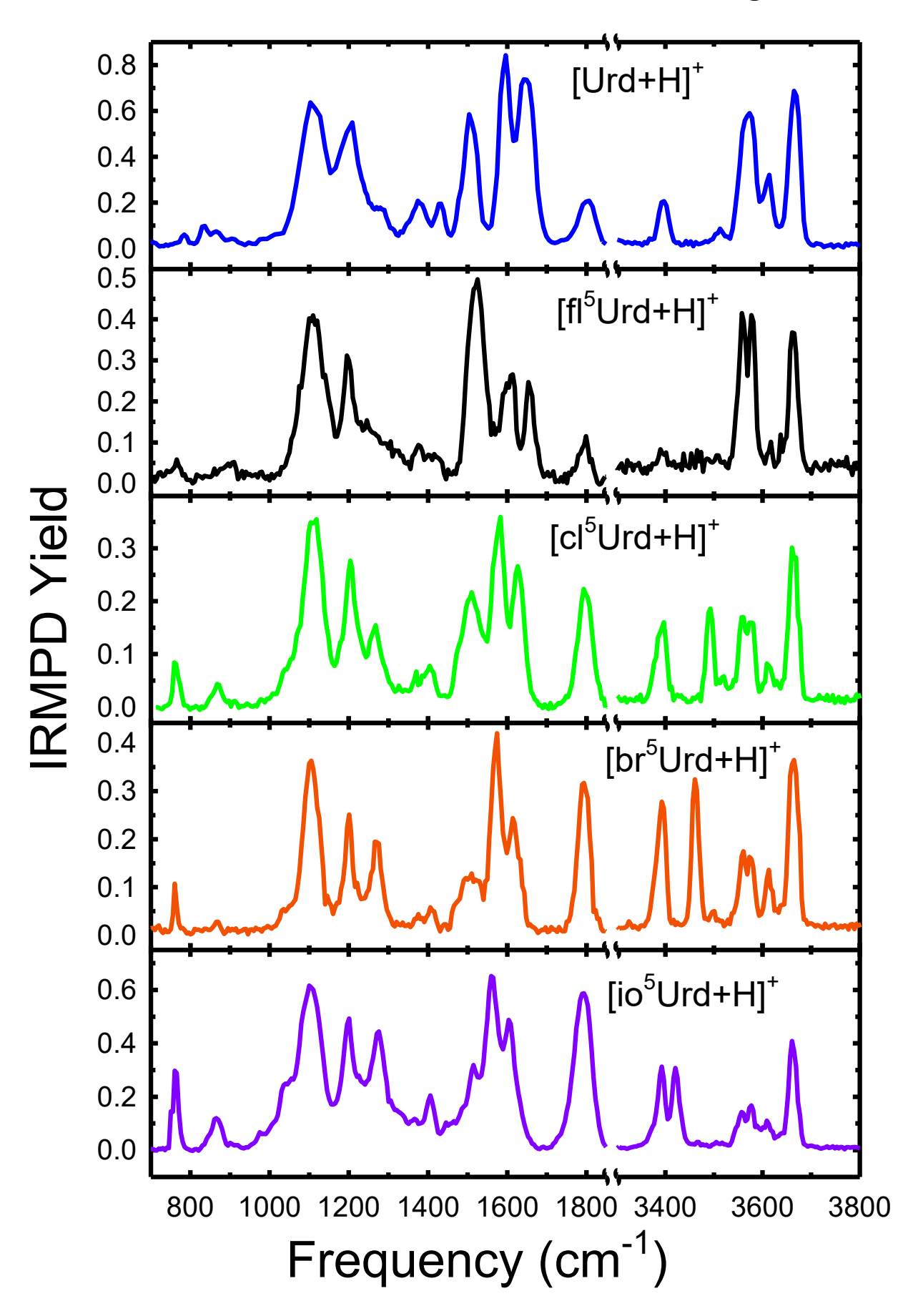
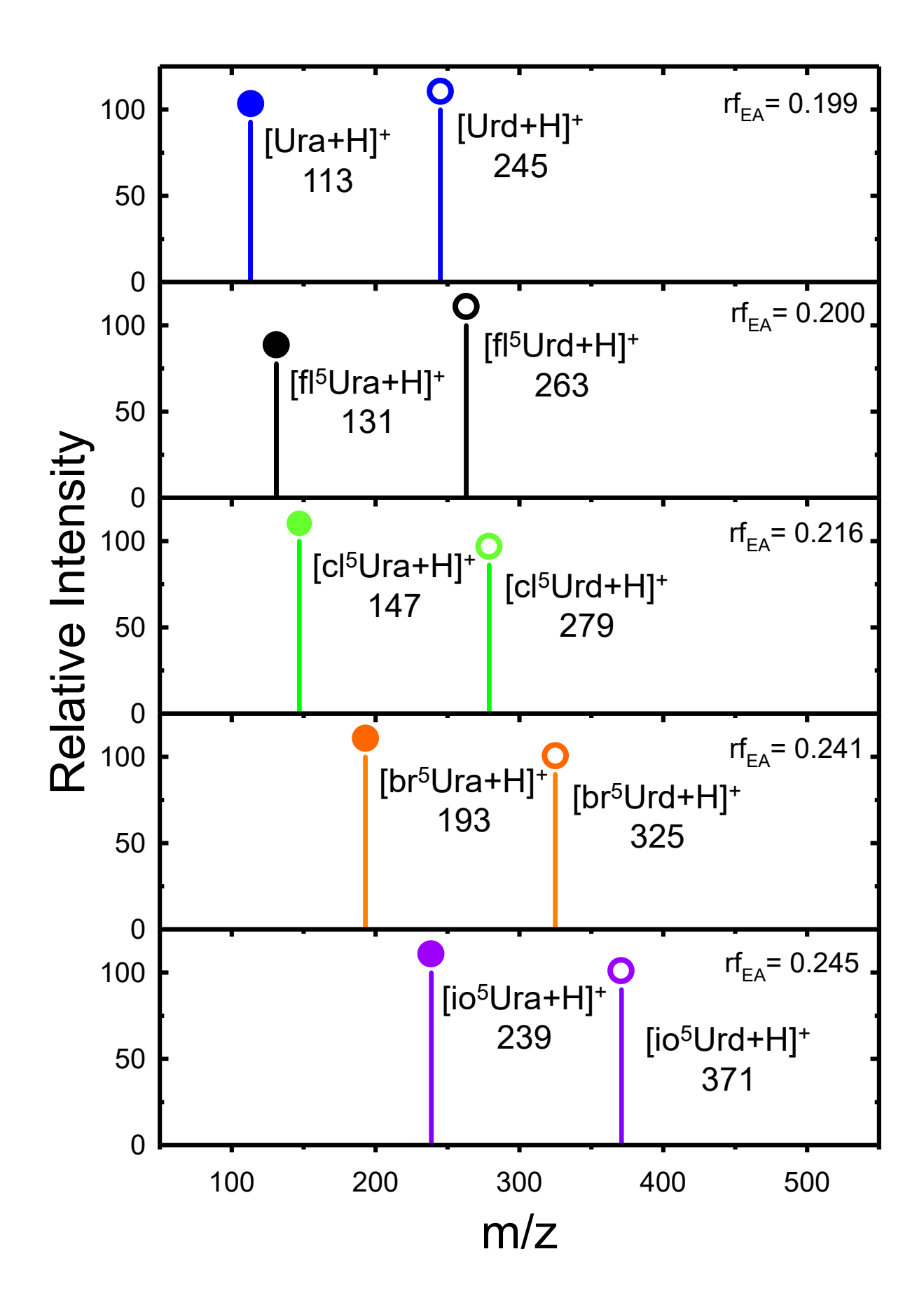


Figure 3.



## Figure 4.

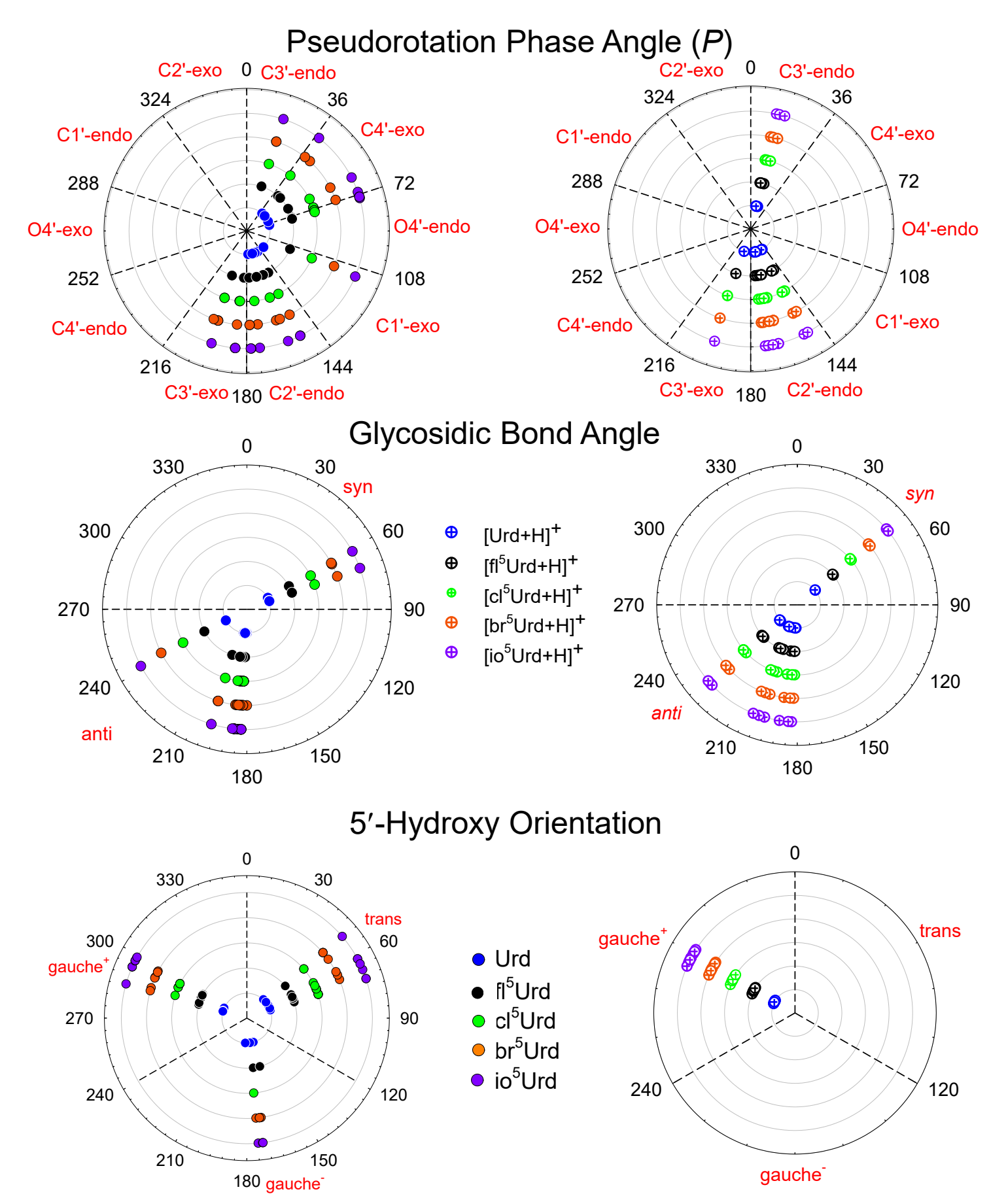
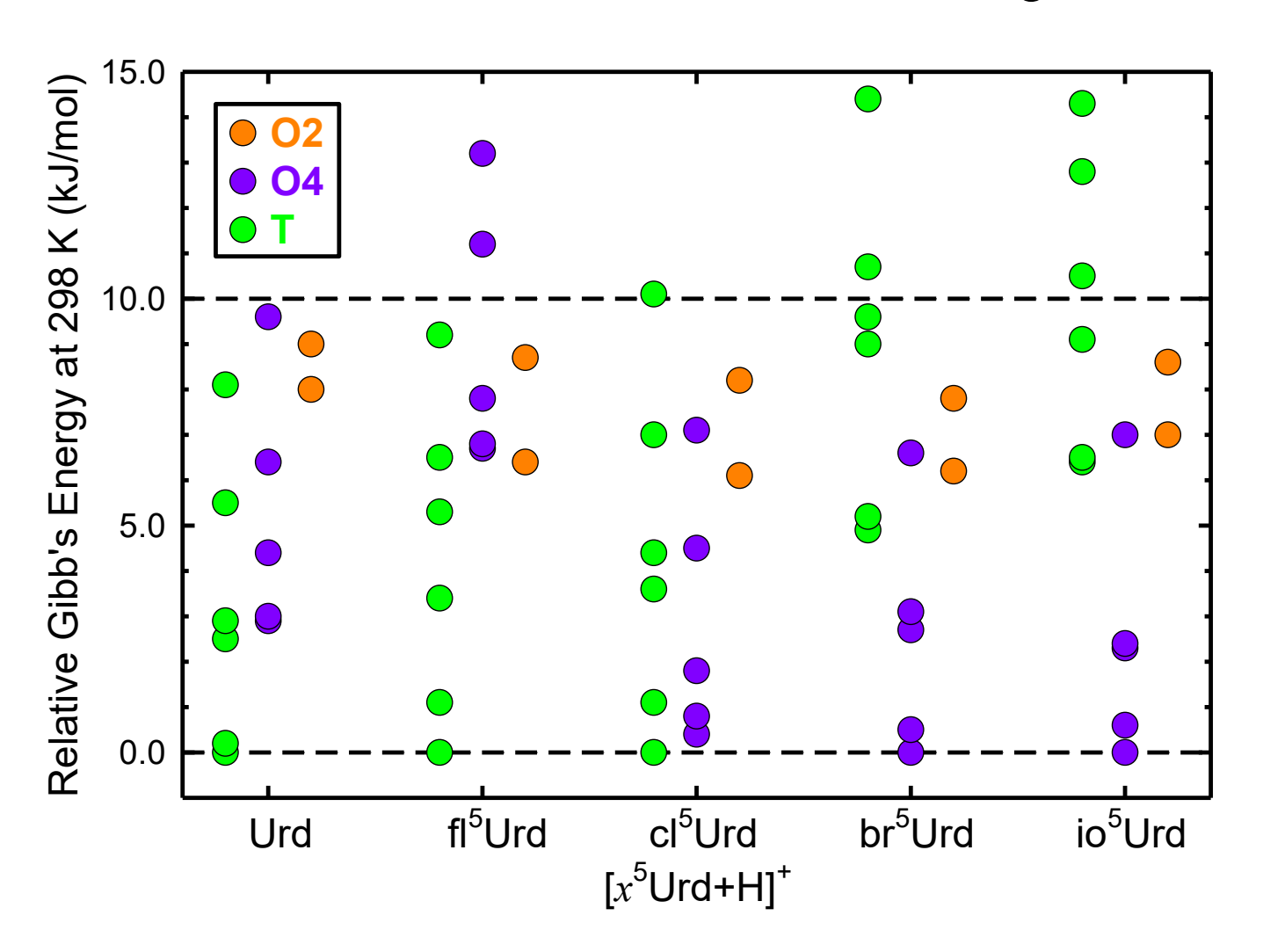
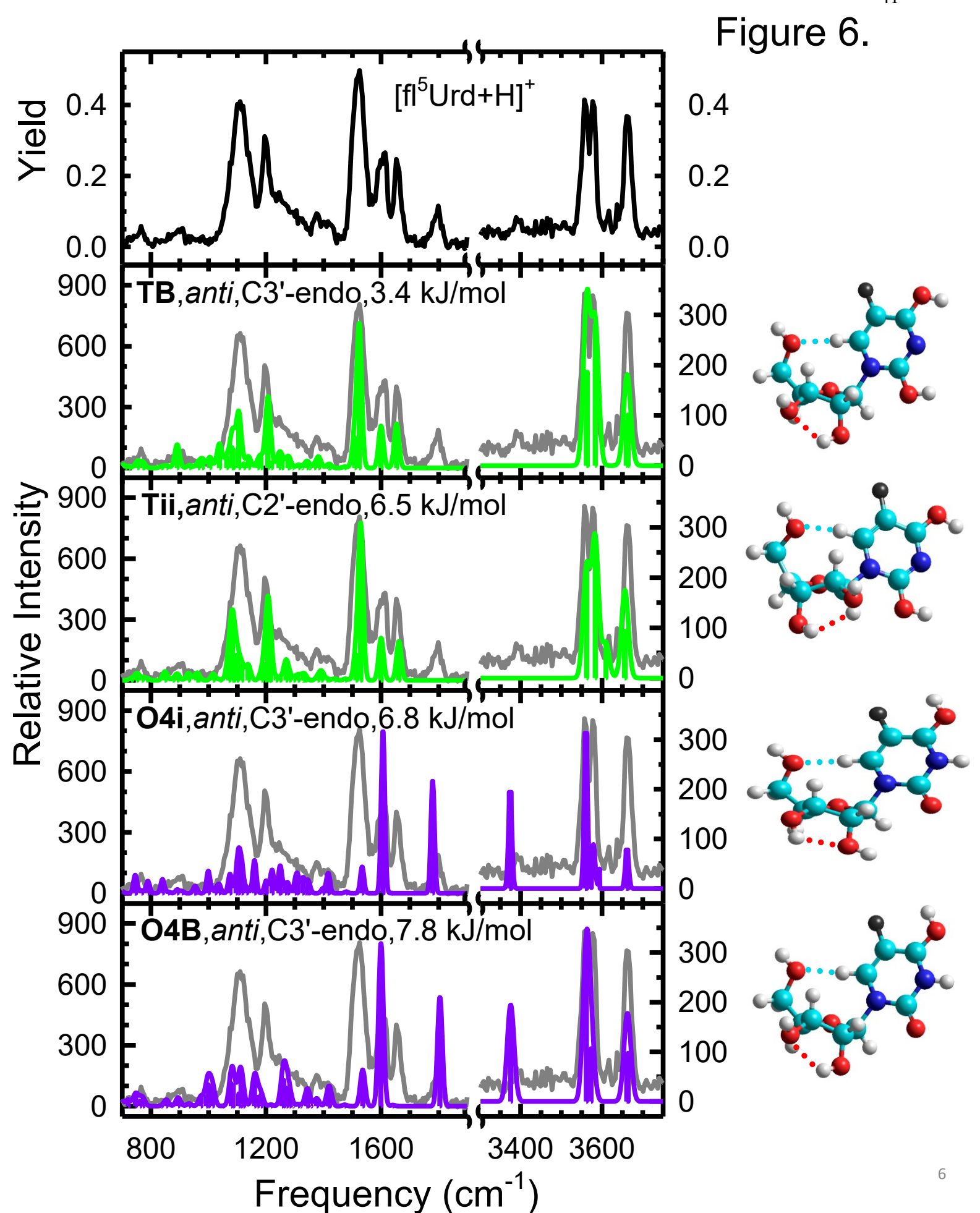


Figure 5.





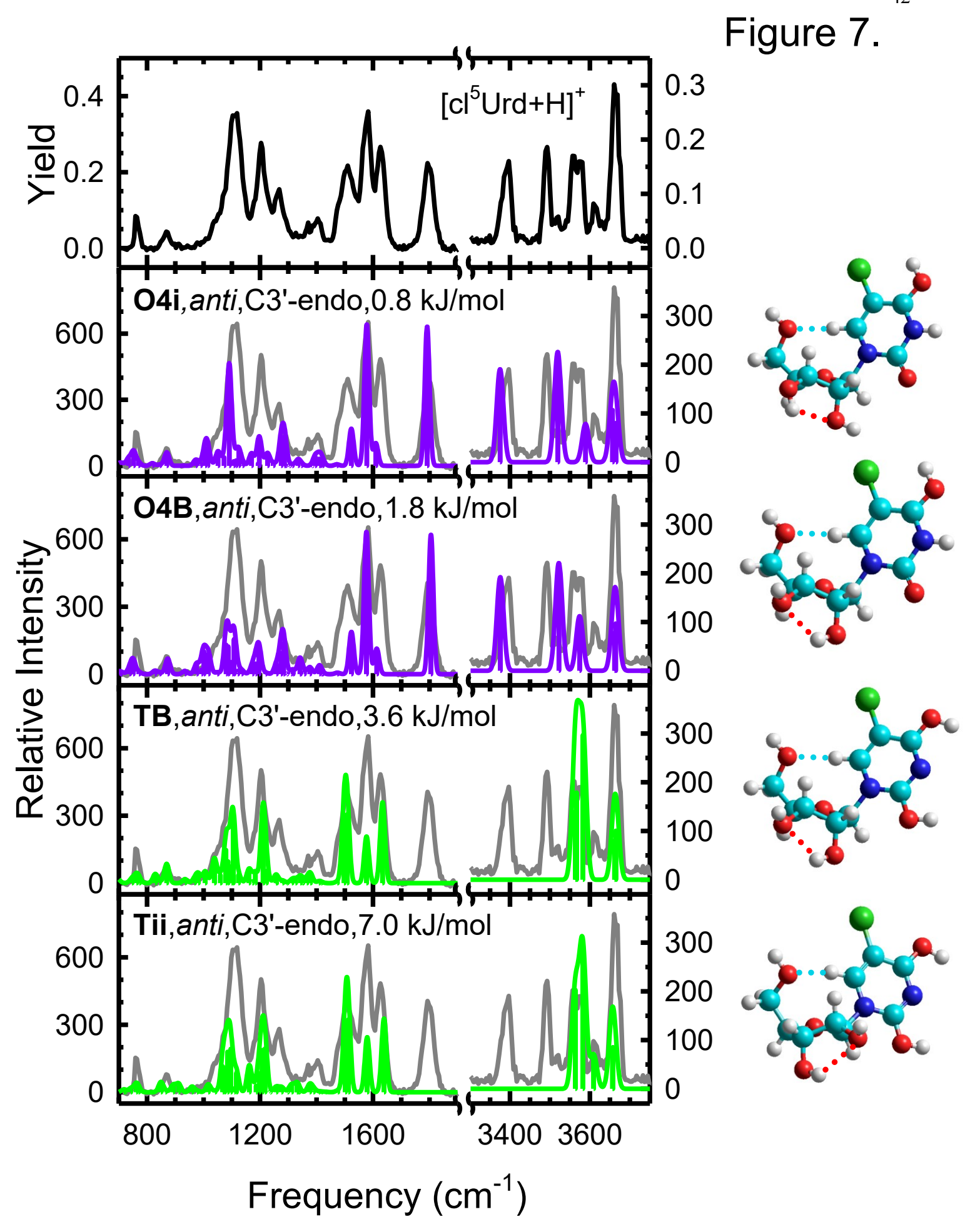
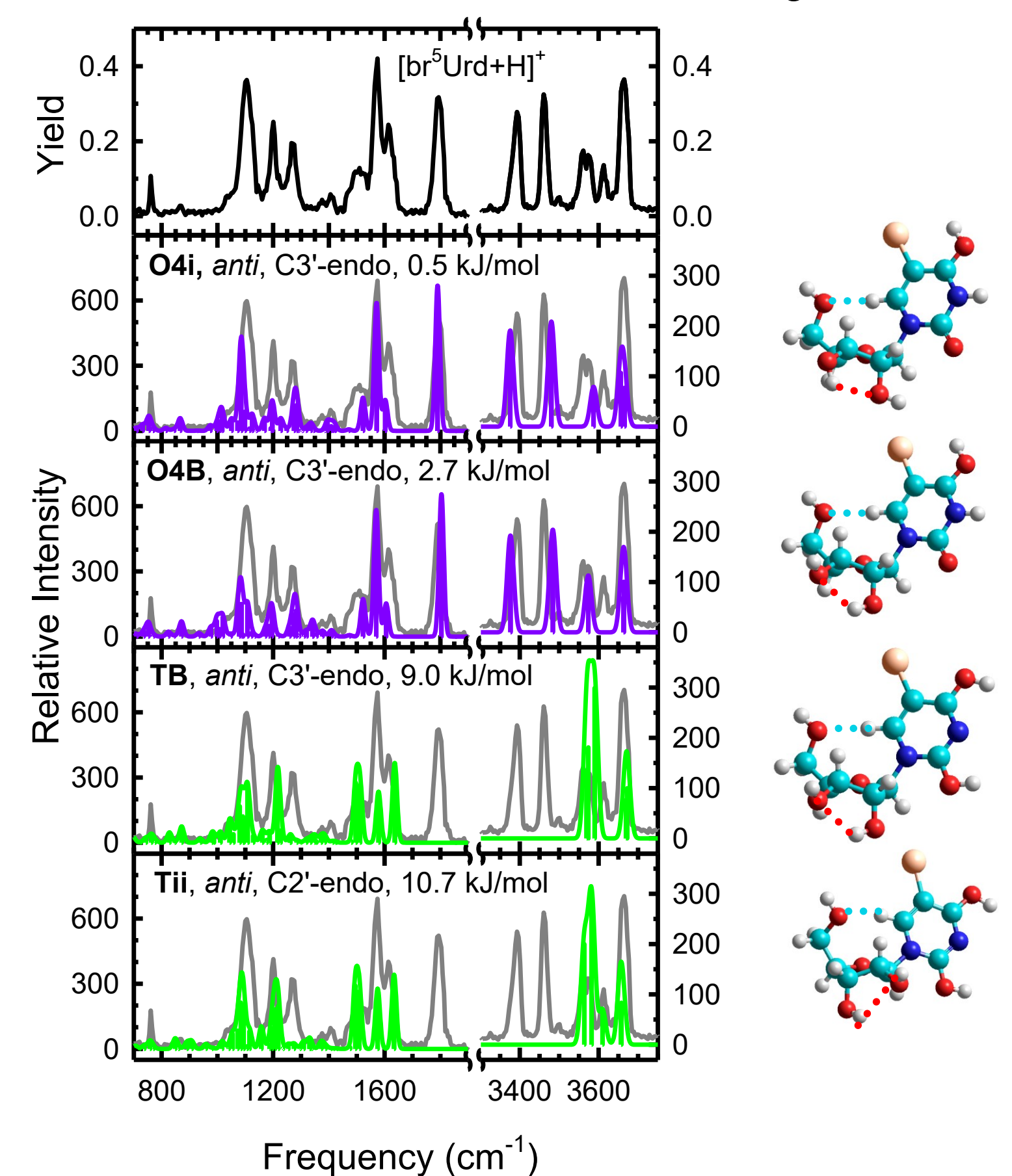


Figure 8.



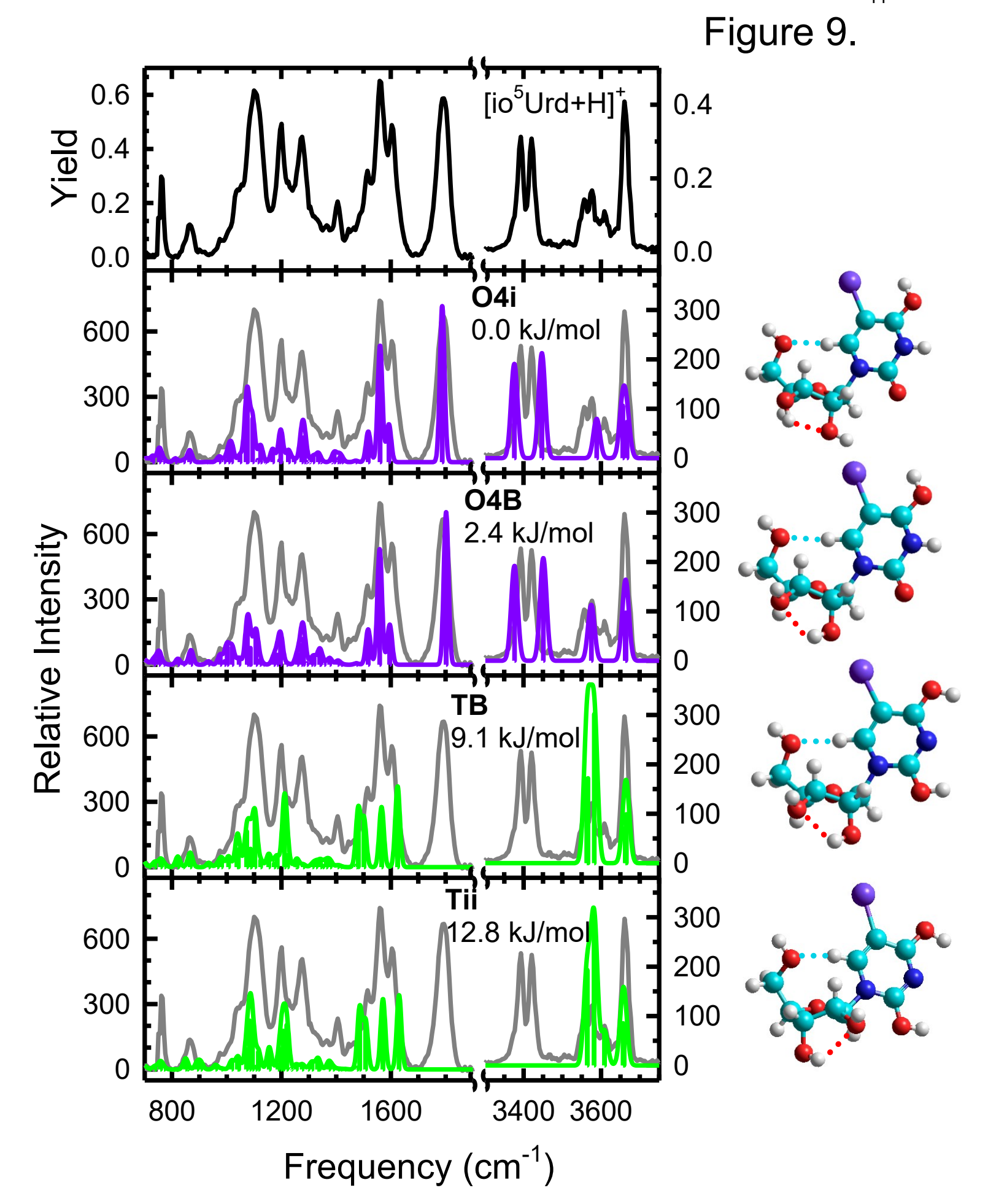
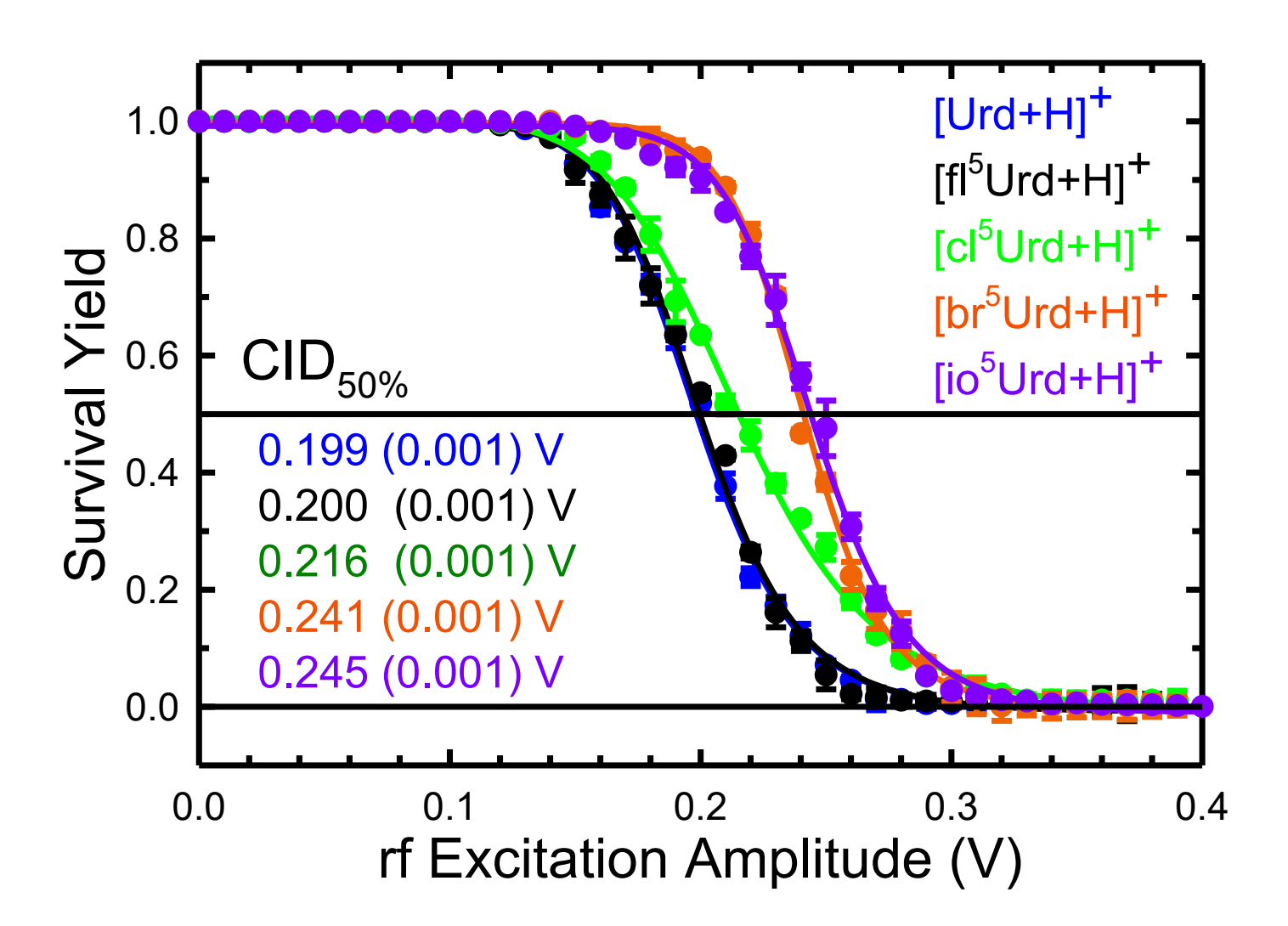
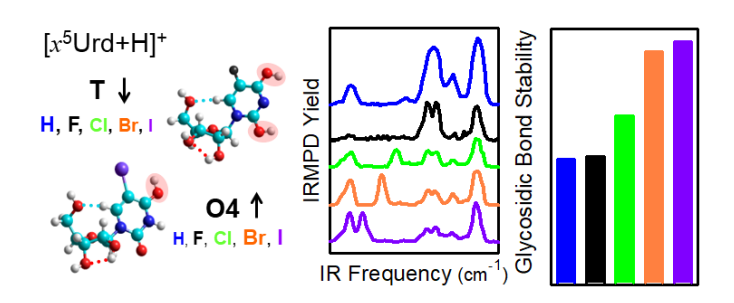


Figure 10.



## For Table of Contents Use Only



# 5-Halogenation of Uridine Suppresses Protonation-Induced Tautomerization and Enhances Glycosidic Bond Stability of Protonated Uridine: Investigations via IRMPD Action Spectroscopy, ER-CID Experiments, and Theoretical Calculations

Neven M. Mikawy, H. A. Roy, Z. Israel, L. A. Hamlow, Y. Zhu, G. Berden, J. Oomens, and M. T. Rodgers\*

The influence of 5-halogenation of the structure and glycosidic bond stability of the protonated form of the canonical RNA nucleoside, uridine, is examined using complementary IRMPD action spectroscopy and energy-resolved collision-induced dissocation experiments and computational methods. 5-Halogenation is found to suppress protontion-induced tautomerization of uridine and enhance glycosidic bond stability.